TRIBHUVAN UNIVERSITY
INSTITUTE OF ENGINEERING
PULCHOWK CAMPUS

B-09-BAS-2019/24

DEVELOPMENT OF HYBRID CROSS-CORRELATION AND OPTICAL FLOW METHOD FOR BACKGROUND ORIENTED SCHLIEREN

By:

Nimesh Chaulagain (076BAS022)

Samiksha Dhakal (076BAS033)

Shushant Poudel (076BAS042)

Sushil Pandey (076BAS044)

A PROJECT TO THE DEPARTMENT OF MECHANICAL AND AEROSPACE ENGINEERING IN PARTIAL FULFILLMENT OF THE REQUIREMENT FOR THE BACHELOR'S DEGREE IN AEROSPACE ENGINEERING

DEPARTMENT OF MECHANICAL AND AEROSPACE ENGINEERING
LALITPUR, NEPAL

MAY 3, 2024

COPYRIGHT

TRIBHUVAN UNIVERSITY

INSTITUTE OF ENGINEERING

PULCHOWK CAMPUS

DEPARTMENT OF MECHANICAL AND AEROSPACE ENGINEERING

The undersigned certify that they have read, and recommended to the Institute of Engineering for acceptance, a project report entitled "DEVELOPMENT OF HYBRID CROSS-CORRELATION AND OPTICAL FLOW METHOD FOR BACKGROUND ORIENTED SCHLIEREN" submitted by Nimesh Chaulagain, Samiksha Dhakal, Shushant Poudel and Sushil Pandey in partial fulfillment of the requirements for the degree of Bachelor of Aerospace Engineering.

Supervisor:
Asst. Prof. Kamal Darlami
Department of Mechanical and Aerospace Engineering

External Examiner:
Ashish Manandhar
MPC Engineer
Himalaya Airlines

Tribhuvan University
Institute of Engineering
Department of Mechanical and Aerospace
Pulchowk

Head of Department:
Asst. Prof. Sudip Bhattrai (Ph.D.)
Department of Mechanical and Aerospace Engineering

DATE: 12th March 2024

ABSTRACT

Flow visualization is one of the most active fields of research in fluid dynamics. The BOS technique is a modern measurement technique aimed at obtaining quantitative data based on variations of refractive index in optically transparent fluids. Flow parameters can be measured with a simple experiment configuration with the help of this technique. This project aims to develop a hybrid algorithm combining cross-correlation with an optical flow algorithm that lends itself to an efficient algorithm that extracts the data accurately. A test setup was built for image acquisition for testing of the algorithm. Chronos 2.1 high-speed camera and iPhone 11 mobile phone were used to obtain image data from experiments conducted with a thermal plume from a candle as a unit test subject and an under-expanded jet from a nozzle as the main test subject. The project successfully demonstrated the efficacy of the hybrid cross-correlation and optical flow algorithm in the context of BOS. By integrating these techniques, the project introduced a novel approach to quantitative flow measurement, showcasing its accuracy and reliability in obtaining precise measurements.

Key Words: *BOS, Cross-Correlation, Flow Visualization, Optical Flow, Speckle Pattern*

ACKNOWLEDGEMENT

With sincerity, we would express our sincere gratitude to our project supervisor Asst. Prof. Kamal Darlami, Deputy Head of Department, Department of Mechanical and Aerospace Engineering for his guidance, support and inspiration throughout this study. We would also like to express our sincere gratitude towards the Department of Mechanical and Aerospace Engineering, Institute of Engineering for providing us the opportunity to carry out the project as a partial fulfillment of the requirements for the Bachelor's Degree of Aerospace Engineering. We are also thankful towards Asst. Prof. Dr. Sudip Bhattrai, Head of Department, Department of Mechanical and Aerospace Engineering for his constant encouragement and words of wisdom. We would also like to acknowledge the Incubation, Innovation and Entrepreneurship Center, Institute of Engineering, for providing us with the working space for conducting experimental works of background-oriented schlieren setup. Special thanks to Mr. Salim Maharjan and Mr. Anup Pandey for their unwavering support and for providing guidance to us while working in background-oriented schlieren setup.

Authors:

Nimesh Chaulagain (076BAS022)

Samiksha Dhakal (076BAS033)

Shushant Poudel (076BAS042)

Sushil Pandey (076BAS044)

TABLE OF CONTENTS

LIST OF FIGURES

LIST OF TABLES

LIST OF ABBREVIATIONS

2D	Two-Dimensional
3D	Three-Dimensional
BOS	Background Oriented Schlieren
CD	Converging-Diverging
CAD	Computer Aided Design
CFD	Computational Fluid Dynamics
DCC	Discrete Cross-Correlation
DFT	Discrete Fourier Transform
FDM	Finite Difference Method
FEM	Finite Element Method
FVM	Finite Volume Method
IA	Interrogation Area
PIV	Particle Image Velocimetry
RHS	Right Hand Side

CHAPTER 1: INTRODUCTION

1.1 Background

An important aspect of fluid mechanics is studying the patterns produced by flowing fluids for the purpose of understanding them. Fluids, such as air and water are transparent in nature. Thus, their flow patterns are invisible entailing the need of some special techniques to make them visible.

Flow visualization and measurement techniques like traditional schlieren, shadowgraph, and interferometry techniques have been used in mechanical and aerospace applications for several years now. These techniques rely on the change in the refractive index as an indicator of flow density and temperature variations. Although schlieren and shadowgraph were once thought to be qualitative visualization methods lacking quantitative power, various research is being conducted in these areas to derive more quantitative information.

Due to the need for an expensive optical setup, limited field of view and cost the use of these traditional techniques is limited to the investigation of small or medium-sized fields of view confined within the laboratory setting only. Except for a few cases (e.g. [4] ,[5]) the applications of these techniques are confined to small-scale laboratory experiments or to wind tunnels and have less feasibility for full-scale outdoor applications. This posed a big problem since most of the aerodynamic flow phenomena are exceedingly difficult to simulate in laboratories. Phenomena such as oblique shock waves formed by the supersonic aircraft or the wing tip vortices from the helicopter's blade could not be replicated in laboratories, whose detailed study is nonetheless crucial.

These limitations paved the way for the Background Oriented Schlieren (BOS) which is one of the most recent developments in the field of flow visualization. This new approach is based on the image processing of the flow field taken from a high-resolution camera. BOS allows visualization of density changes easily without using complex optical equipment. The above-mentioned technique uses a background image as a reference image to detect disturbance and its process requires the detection of the distortions due to measurement medium relative to the reference image as shown in figure 1.1.

Refraction causes deviation in the paths of the rays i.e. distortion of the image. Refraction will create an optical contribution by causing distortion in the captured image. This distortion is then used to determine the refractive index gradient. The change in the refractive index due to the test field is then calculated and is related to the density gradient using the Gladstone-Dale equation. This new technique has been successfully applied not only to supersonic jets and flames but also to a helicopter in hovering flight. Due to the need for a simple optical setup, it can be used for the quantitative measurement of the flows from low subsonic indoor airflow [6] to hypersonic flows [7].

From the image processing point of view, the BOS method uses a procedure called the principle of cross-correlation like that of PIV in which seeder particles are used for the flow visualization, on the other hand BOS uses the background pattern, which consists of random dots, behind the test section. Though, similar BOS images have some stark differences with the PIV images, in terms of the particle size and the particle displacement. There have been limited attempts to implement the image processing algorithm designed specifically for BOS and to gather the flow information.

The two commonly used algorithms for displacement field measurements are cross-correlation and the optical flow algorithm. The cross-correlation method captures displacement by analyzing the correlation between particles within a defined window, providing an averaged displacement of the particle cluster. This method effectively yields one velocity vector per window, determining the spatial resolution of the velocity field. On the other hand, the optical flow method employs a differential strategy, computing the time derivative and spatial gradient of image intensity fields. It operates under the constraint that displacements must remain smaller than the characteristic length scale of discernible features within the image plane.

The cross-correlation method has a disadvantage in that the size of the interrogation window must not be too small to get reliable and accurate results. This limits the spatial resolution of the result obtained and prevents detection of the small pixel displacements [8].

The optical flow algorithm on the other hand becomes effective when the speckle displacement is smaller than the size of the speckle, which corresponds with the phase object with a low refractive index gradient, on the other hand if the displacements of particles are much larger than their sizes, temporal and spatial differentiation of the

image intensity cannot be calculated accurately [9]. Thus, rendering the measurement inaccurate in the case of the phase field with a high refractive index gradient.
One way to overcome this problem is to implement the optical flow method with that of the cross-correlation method. Though the method has not been implemented in the case of the BOS, the hybrid algorithm is found to consistently give improved results at least in case of the PIV [9].

1.2 Optical Principle of Background Oriented Schlieren

The BOS is governed by the variation of the refractive index due to the density gradient in the presence of non-homogeneous field. The fundamental relationship between density gradient and variation of refractive index is given by the Gladstone-Dale equation as follows.

$$n - 1 = G(\lambda)\rho \tag{1.1}$$

Where,

n : refractive index of the medium

ρ : density of the medium (kg/m^3)

$G(\lambda)$: Gladstone-Dale constant

The Gladstone-Dale constant is a function of the wavelength λ as well as that of the medium. The constant $G(\lambda)$ can be calculated to be $0.23 \times 10^{-3}\,\mathrm{m}^3/\mathrm{kg}$ for air. The above equation shows a linear relationship between the refractive index of the medium and the density of the medium.
The Schlieren theory states that "the deflection angle of light due to an non-homogeneous flow field is a line integral of the refractive index gradient $\frac{\partial n}{\partial y}$ along the optical axis z". The Schlieren equation can be written as follows:

$$\epsilon_y = \frac{1}{n}\int \frac{\partial n}{\partial y}\, dz \tag{1.2}$$

A typical BOS setup consists of basic optical components such as a camera and a background image which is also called a speckle pattern as shown in figure 1.1.

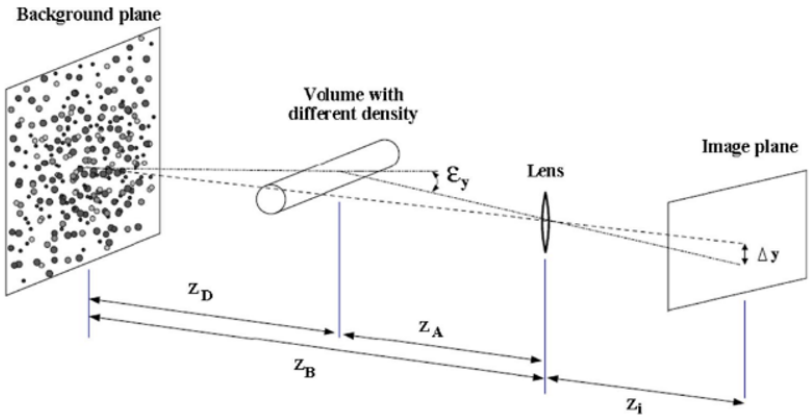

Figure 1.1: Optical Configuration of BOS

The principle of BOS technique can be shown as follows in figure 1.2.

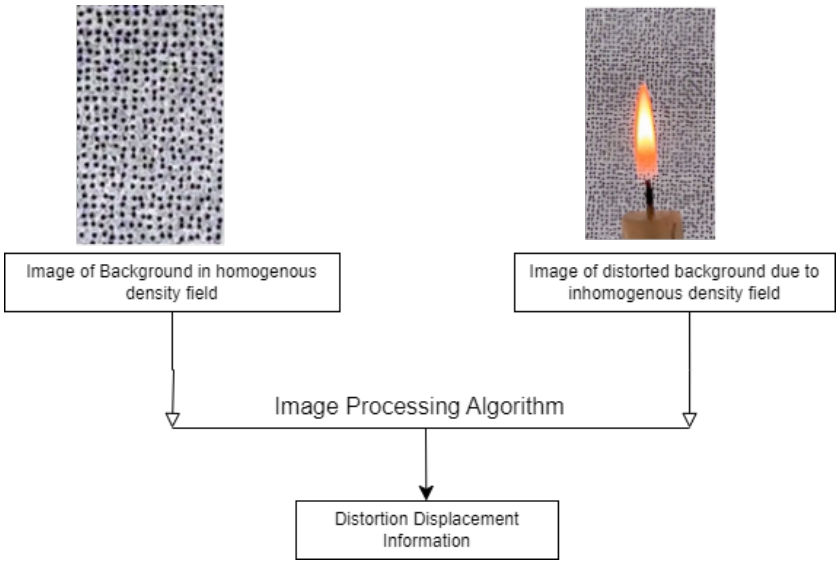

Figure 1.2: Technical Principle of BOS

In this technique first a reference image, which is the image of the background pattern without flow field interference, is recorded. The background image is again recorded in the presence of flow field interference. This image is called the distorted image. Then the displacement of the corresponding particles in the two images can be processed by using a cross-correlation algorithm or optical flow algorithm. These algorithms are written using a programming language such as MATLAB to provide information on the refraction of light due to the presence of the density gradient.

The deflection of the light in the non-homogeneous field results in displacement ob-

served in the speckle patterns relative to those in the reference image can be understood as density gradients along the optical path. This displacement, when analyzed using the Gladstone-Dale equation, allows for the interpretation of integrated density gradients. It's apparent that from the two-dimensional density gradient, one can derive an approximation of the density through integration.

The displacement of the image (Δy) can be obtained for the BOS technique, assuming paraxial recording and small angle deflections, as follows:

$$\Delta y = Z_D \cdot M \cdot \epsilon_y \tag{1.3}$$

Where,

Z_D : distance of background pattern from the non-homogeneous field

M : magnification factor of the background $= \dfrac{Zi}{Z_B}$

ϵ_y : deflection angle

Dalziel et al. [10] discussed the sensitivity of the technique in terms of varying distances between the background pattern, the non-homogeneous flow field, and the camera. They outlined how an increase in distance Z_D enhances the sensitivity of the system, while the distance $Z_D - Z_i$ is adjusted to maintain focus of the image. To prevent perspective distortion the camera must be placed as far from the test section as possible. In BOS techniques, the background and the test object are placed such that both can be focused properly by the camera. The flow field under investigation is on the viewing axis. Due to the change in the refractive index, the dot patterns in the background will be displaced compared to the reference frame. The unknown lensing effects and the finite depth of field, and the strength of the refractive media, makes it difficult to keep both the object and the background in sharp focus. Various factors such as camera sensor quality and the algorithm affect the quality of the results.

Some simplifying assumptions are made that allow approximating the test field as a point instead of a volume [11]:

- No refraction occurs outside of the medium being imaged as the surrounding medium is uniform.
- The distance between the camera and the background is large in comparison to the overall size of the field.

1.2.1 Measurement of non-homogeneous Density Fields using BOS

BOS is a non-intrusive quantitative optical flow measurement technique used to determine density variations due to non-homogeneous fields. In addition to this, BOS has been quite often used in the measurement of temperature field and other flow parameters such as velocity structure in the flow field. The density of the gases in the presence of non-homogeneous fields can be determined by solving Poisson's equation [12].
Poisson's equation is an elliptic partial differential equation formed by the derivative of the refractive index gradients. The displacement vector field is further integrated to calculate the refractive index [13].
The Poisson's equation is given by:

$$\frac{\partial^2 n}{\partial x^2} + \frac{\partial^2 n}{\partial y^2} = R\left(\frac{\partial \Delta x(x,y)}{\partial x} + \frac{\partial \Delta y(x,y)}{\partial y}\right) \tag{1.4}$$

Where,

n : local refractive index

Δx : displacement in the x direction

Δy : displacement in the y direction

R : constant from geometrical setup

1.3 Image Processing Algorithms

1.3.1 Cross Correlation Algorithm

The cross-correlation algorithm is comparable to the pattern-matching technique, as such it can be understood as the statistical pattern-matching technique in which a pattern of speckles is found from interrogation window A in interrogation window B. Mathematically, the operation involved in cross-correlation is similar to that of convolution with the exception that correlation provides the degree to which the two signals (in our case images) are similar. The operations involved in convolution are similar to cross-correlation except for the folding operation which is not performed in cross-correlation. Typically, both the reference (image without density field) and distorted image (image

with density field) are sub-divided into interrogation areas which are referred to as the interrogation windows [1]. Once the images have been divided an average displacement vector is determined by maximizing the cross-correlation function. The discrete cross-correlation function is defined as

$$C(m,n) = \Sigma_i \Sigma_j A(i,j) B(i-m, j-n) \tag{1.5}$$

where A and B are the interrogation areas from window reference and distorted images respectively.

The location at which the maximum correlation intensity, also referred to as correlation peak, is achieved will be the most probable location of the displaced pixels. There are two approaches to solving equation (1.5) one is to compute directly in the spatial domain and the other is to compute in the frequency domain [14].

The first approach is referred to as the direct cross-correlation (DCC) [15] while the other approach is referred to as the discrete Fourier transform (DFT) [16]. Figure 1.3 illustrates the two ways of determining the correlation function, the upper half of the figure shows the DCC technique while the lower half of the image shows DFT technique.

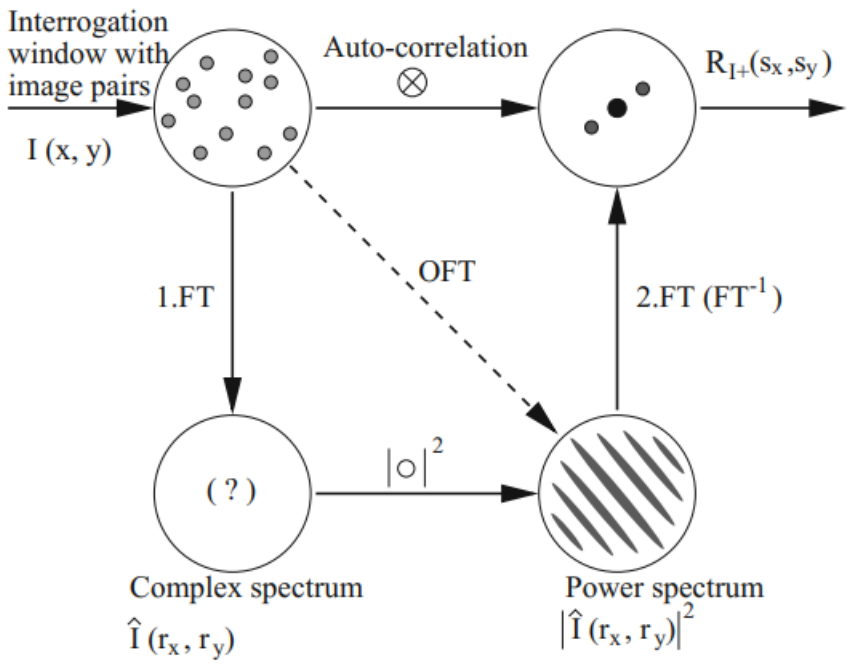

Figure 1.3: Comparison of the method of determining correlation function using DCC and DFT [1]

Despite the simplicity of equation (1.5) it cannot be directly used since cross-correlation function obtained is sensitive to the intensity change. This difficulty is counteracted by normalizing the equation (1.5). After normalizing equation (1.5) we get following [14]

$$R(m,n) = \left\{ \sum_i \sum_j [A(i,j) - A'] \times [B(i-m, j-n) - B'] \right\} \times \left\{ \sum_i \sum_j [A(i,j) - A']^2 \times \sum_i \sum_j [B(i,j) - B']^2 \right\}^{-1/2} \tag{1.6}$$

Here, A' and B' are the mean intensities of A and B respectively. Clearly, implementation of the equation (1.6) in the frequency domain is more involved than implementing it in the spatial domain.

Sub-Pixel Accuracy

The maximum value of the discrete correlation function is an integer peak. The accuracy of the computation rests on determining the correlation peak more accurately. For this purpose, sub-pixel accuracy is used. Sub-pixel accuracy is used to localize the position of an object (in our case interrogation window) within an image with precision finer than the size of the pixel.

Different interpolation techniques are available for sub-pixel image interpolation [17]. Evaluated different interpolation methods for PIV application these include linear, quadratic, truncated sinc, windowed sinc, cubic, Lagrange, Gaussian 2^{nd} and 6^{th} interpolators. Among the many available options, Gaussian curve fitting is the most frequently used. Assuming the integer peak is at (x_o, y_o) in a correlation function $R(m,n)$, then the accurate location of the correlation peak is calculated by the following equation [14].

$$\begin{aligned} x &= x_0 + \{logR(x_0 - 1, y_0) - logR(x_0 + 1, y_0)\} \\ &\times \{2[logR(x_0 - 1, y_0) + logR(x_0 + 1, y_0) - 2logR(x_0, y_0)]\}^{-1} \\ y &= y_0 + \{logR(x_0, y_0 - 1) - logR(x_0, y_0 + 1)\} \\ &\times \{2[logR(x_0, y_0 - 1) + logR(x_0, y_0 - 1) - 2logR(x_0, y_0)]\}^{-1} \end{aligned} \tag{1.7}$$

1.3.2 Optical Flow Algorithm

The pixel intensity in the first image at a time t is given by $I(x, y, t)$, and the intensity in the second image taken after time dt is postulated as $I(x + dx, y + dy, t + dt)$.

$$I(x, y, t) = I(x + dx, y + dy, t + dt) \tag{1.8}$$

where $I(x, y, t)$ is image intensity as a function of space (x, y) and time t.

Optical flow, in the context of analyzing two sequential images, refers to the two-dimensional vector field that describes the perceived movement of individual pixels between frames of a dynamic three-dimensional scene captured at distinct moments in time[11]. The underlying principle of optical flow principle is that it employs the assumption of brightness constancy. To put in other words, assumption of brightness constancy means that pixel intensity for corresponding 3D points is the same in both images as given by equation (1.8).

Optical flow employed in Background-Oriented Schlieren (BOS) applications often lacks distinct abrupt changes but may include high-frequency details spread widely, particularly in turbulent flow imaging scenarios. In contrast, when dealing with optical flow in three-dimensional scenes, the consistency of brightness is compromised in the presence of shadows and foreground objects obstructing the background. Additionally, the strict adherence to brightness constancy is seldom achieved, as the fundamental assumption relies on the stability of surface radiance between consecutive frames.

$$\frac{\partial I(x, y, t)}{\partial x}\frac{dx}{dt} + \frac{\partial I(x, y, t)}{\partial y}\frac{dy}{dt} = -\frac{\partial I(x, y, t)}{\partial t} \tag{1.9}$$

where $I_x = \frac{\partial I(x,y,t)}{\partial x}$, $I_y = \frac{\partial I(x,y,t)}{\partial y}$, and $I_t = \frac{\partial I(x,y,t)}{\partial t}$ denote spatial and temporal partial derivatives of the image I.

Ignoring higher-order terms in the Taylor series and then substituting the linear approximation

$$\frac{\partial I(x, y, t)}{\partial x}\frac{dx}{dt} + \frac{\partial I(x, y, t)}{\partial y}\frac{dy}{dt} = -\frac{\partial I(x, y, t)}{\partial t} \tag{1.10}$$

Here, the image velocity or optical flow is given by $\frac{dx}{dt} = u$ and $\frac{dy}{dt} = v$. Equation (1.10) relates the velocity to the space-time image derivatives at one image location and is often called the gradient constraint equation [18]. The fundamental optical flow framework serves as a suitable model for understanding refraction in Background Ori-

ented Schlieren (BOS) imaging. Specifically, the principle of brightness constancy (as indicated in equation (1.8)) remains valid for typical flows of interest, provided the BOS setup is meticulously engineered. Notably, brightness constancy relies on certain assumptions, which are crucial considerations in BOS imaging:

1. flow is transparent and non-scattering
2. density gradients within the flow are minimal
3. stable lighting from sources
4. small camera aperture

Addressing these assumptions diligently is essential for accurate BOS imaging.

Horn and Schunck Algorithm

The Horn-Schunck optical flow method is a gradient-based algorithm designed to detect the motion of light intensity between a pair of images. This approach, outlined in reference [19], incorporates a smoothness constraint, positing that each point within the image experiences a comparable displacement to its neighboring points. The recovery of optical flow from one gradient constraint is not possible since equation (1.10) is one equation with two unknowns, u and v.

Horn and Schunck proposed an energy functional for global smoothing.

$$E(\mathbf{w}) = \int_1 \left((\nabla I \cdot \mathbf{w} + I_t)^2 + \lambda \left(\|\nabla u\|^2 + \|\nabla v\|^2 \right) \right) \, dxdy \tag{1.11}$$

Here, $\mathbf{w} = (u, v)$. The energy functional minimizes the difference between image gradients and flow. This provides the advantage of enabling information propagation over large distances in the image.

Components:

- Spatial gradients of the flow (u and v)
- Image gradients (∇I) and temporal gradients (I_t)
- Regularization term for smoothness (λ)

Objective: Minimization of the energy functional through optimization.
Optimization Method:

- Discrete approximations used for solving.
- Large system of linear equations solved iteratively (e.g., Gauss-Seidel, Successive Over-Relaxation).

In equation (1.11), the Horn and Schunck optical flow method incorporates a smoothing parameter, denoted as λ, which is set equal to the expected noise level present within the image. This choice of λ aims to minimize errors, particularly in regions with small brightness gradients. The selection of λ is user-defined and tailored to meet specific requirements. To compute the displacement, the method initially estimates the partial derivatives of brightness at each point within the image along both the horizontal (x) direction (denoted as (I_x) and the vertical (y) direction (denoted as (I_y)). Subsequently, discrete approximations yield a large system of linear equations, which is then solved through iterative techniques.

1.4 Problem Statement

Most of the flow visualization techniques that are currently available (schlieren, shadowgraph etc.) only provide qualitative information about the flow. The information obtained from these techniques, though valuable, is not sufficient to understand the flow completely. Furthermore, measurement techniques are intrusive in nature and affect the flow itself. This results in inaccurate measurement of parameters of the flow. BOS has advantages to circumvent these drawbacks.
However, a program designed specifically for the BOS analysis has not been developed yet showing great gap in application of BOS in flow visualization and measurement. Though the combination of the optical flow and cross-correlation algorithm has been studied for PIV it has not been studied and implemented in the case of BOS. This project aims to develop a hybrid method combining optical flow and cross correlation algorithm designed specifically for BOS processing and build a setup to measure several types of flow variables using the developed algorithm.

1.5 Objectives

1.5.1 Main Objective

The objective of this project is to develop a hybrid cross-correlation and optical flow method designed specifically for the BOS implementation.

1.5.2 Specific Objectives

1. Implement the hybrid method for measuring a parameter of flow i.e. density.
2. Build adequate image acquisition setup for BOS to check the feasibility in cases of high and low-density gradients.

1.6 Scope of the Work

As the current project focuses on the development of a hybrid BOS data processing algorithm, the algorithm and the test setup can be used for any quantitative measurement of any flows that produces a sufficiently detectable refractive index gradient. Allowing for the non-intrusive measurement of different parameters for any kind of fluid flow.

1.7 Applications

- The BOS has the ability of qualitative and quantitative measurement of flow parameters in compressible flows, low-speed flows, and convection phenomena.
- BOS allows visualization of turbulent and laminar flows of liquids and gases, acoustic phenomena, such as high-frequency ultrasound, and the chemical composition of the media.
- The algorithm that is built for image processing in BOS can be extended for use in remote sensing and strain measurements as well.

1.8 System Requirements

1.8.1 Hardware Requirements

BOS optical setup is fairly simple setup as shown in figure 1.1. The hardware required for the completion of the project are listed below:

- High-speed camera
- Light source

1.8.2 Software Requirements

As stated in the objectives, the project is majorly based on the development of an algorithm to extract quantitative information from flow. Hence the computing software required to achieve the objectives are as listed below:

- Programming language for development of algorithm: MATLAB
- CAD software for the design of Converging-Diverging Nozzle: CATIA

CHAPTER 2: LITERATURE REVIEW

Principle and application of the background-oriented schlieren method was first described in an article that appeared in "Experiments in Fluids" which described several schlieren and other techniques that the authors first named "synthetic schlieren". The application described in the article was that of the internal waves generated by the oscillating cylinder [10]. Then the article by Raffel et. al in the same journal followed in May of 2000, which utilized a random dot pattern in the background and showed its application to a rotor wake visualization of a helicopter in hovering flight [20].The BOS method developed primarily by Meier has some similarities with the "synthetic schlieren" system, the difference lies in the fact that BOS relies on the distortion of a background pattern due to the field while synthetic schlieren uses matching of a real background grid with a synthetic one in the camera [21] [22].

BOS technique is based upon comparing the image with no density field, called the reference image, and the image with the density field [23]. BOS, when combined with other flow measurement techniques, can be used to study the diverse array of the fluid phenomena. For example, Richard and Raffel combined BOS with the results of density and velocity measurements obtained from transonic wind tunnel, to study the blade vortex interaction of Eurocopter BK117 and large US utility helicopter [20]. Natural backgrounds were also used for rotor tip vortex measurements [24]. BOS method was applied on a cone cylinder with 15° (semi apex angle) and flow at a Mach equals 2.0 to visualize the density field by Venkatakrishnan [25]. Vasudeva used the BOS method to determine the distribution of density field of a heated air jet [13].

Background-oriented schlieren technique has been implemented for 2D visualization of convective indoor air flows. A climate laboratory was setup whose surrounding faces could be heated up without disturbing the airflow. Along with it a conventional BOS setup was utilized which consisted of a structured background, the object under investigation, and a high-resolution camera [6]. Visualization of supersonic flows using BOS was carried out using the Drummond reflected shock tunnel which consisted of a driver filled with helium. A Mach 4 conical nozzle was fitted at the end of the shock tube. Multiple glass windows were setup on both top and bottom of the test volume for the flow visualization [26]. BOS was also used in density measurements of rectangular su-

personic jets where compressed air up to 7 bar released through a nozzle in front of a background created by a random number generator [27].

Another application of BOS technique was presented by Hayasaka to explain the possibility of BOS system to extract information of density gradients in tiny size [28]. The BOS method was used with a laser underwater to investigate the shock wave, by measuring the displacement vectors of local density gradients to obtain the pressure field. Nowadays, 3D Background Oriented Schlieren (3DBOS) has been used to perform experimental analysis of 3D structures of supersonic under-expanded screeching jets. The images were captured with the help of 8 cameras placed on azimuthal arc of $1m$ radius with the center on the jet axis [29]. 3D reconstruction of compressible flows has also been carried out using 12 synchronized cameras setup [30].

Block matching algorithms used in PIV processing software for image processing apply spatial correlation to detect the motion of small rectangular windows from frame to frame. This is also known as cross correlation technique and has been widely studied in case of the PIV . Modern cross correlation techniques to eliminate the drawbacks of the standard cross correlation algorithm have been purposed.Ye and Niu et al studied the factors influencing the errors of PIV cross-correlation algorithm and found that increasing the resolution improved the PIV calculation [31]. Shi et. al. used the modified cross-correction algorithm with wavelet transformation and multi resolution analysis (MCCWM) and found that multi-resolution analysis can improve the spatial resolution and the calculation accuracy [32]. Earl et. al. developed a new and robust version of the 2D cross-correlation method referred to as the fast 2D projection re-projection(f2dr) for time resolved volumetric particle image velocimetry (PIV) data [33].

The same theoretical background of the cross-correlation was used in the early BOS experiments. The cross-correlation algorithm used for the PIV applications was used by Raffel et al for the full scale helicopter vortex characterization [34]. Similarly, many software, which use cross-correlation algorithm, has found its use in many scientific research involving BOS. For example *PIVview2C* was used for the two dimensional visualization of convective indoor air flows [35]. Another commercially available software is *FOLKISPIV*, which was used for the 3D reconstruction of a compressible flow by using 12 synchronized cameras [36].

Although, a significant advancement has been found in the generation of high func-

tioning cross-correlation algorithm, it may not always be the best choice for BOS data processing. As it has been found that cross-correlation algorithm results in loss of resolution, especially when higher BOS sensitivity is desired [12][37]. Hence, the optical flow algorithms were also introduced in BOS, although these algorithms were immature among fluid mechanics researchers. The implementation of optical flow algorithms in relation to BOS was first studied by [11].The authors conducted experiments to test both the gradient-based and variational optical flow methods on both real and synthetic datasets. The algorithms by Horn and Schunck and Lucas and Kanade as well as their multi-resolution, multi-scale variants were implemented. The experiment was conducted on the candle plume and candle lantern. The Horn-Schunck algorithm provided visually superior results and slightly lower error than Lucas-Kanade. Much promising results in the superiority of optical flow algorithm in comparison to cross-correlation algorithm in application of incompressible and compressible flows are given in literatures.

BOS using Horn-Schunck algorithm was implemented to measure the pressure field of a laser-induced underwater shock waves [28]. BOS based on optical flow can be implemented in the in-compressible flows too, since water's small density gradient results in a displacement field, it can be acquired at the spatial resolution of one vector per pixel. The newest application of BOS technique using optical flow was conducted by [38]. BOS measurements were conducted on Mach 3.5 supersonic flows over a Von Karman Ogive and a 10° wedge. In the study, the authors demonstrated the superiority of optical flow over cross-correlation in terms of accuracy and resolvable range of density gradient amplitudes. Considering the positive aspects of both the algorithms, a highly optimized algorithm can be developed for processing of BOS data.

The limitations of the cross correlation algorithm has been long been recognized and technique similar to hybrid algorithm has been used, however displacement between the reference image and distorted image was obtained by using the cross correlation algorithm itself [39]. Combining the cross correlation and optical flow is rather new approach of solving the problem. Liu and Salazar developed an open source software for the PIV application [9] . Yang and Johnson also investigated the use of the hybrid algorithm and showed that for the case of the smaller displacement the relative accuracy of the hybrid algorithm is higher. They also compared the different implementation of

the cross correlation and compared the error for each case [40]. Seong et. al. also used global optical flow based on the image warping and showed that the method surpasses the conventional PIV technique in capturing small-scale vortex and turbulent structures owing to its improved spatial resolution [41]. Regardless of all these promising study the implementation of the hybrid algorithm in case of BOS has been limited.

BOS, a non-intrusive optical technique has gained popularity for its versatility and simplicity. Researchers have recognized the potential of incorporating BOS to enhance the visualization of shock waves and other flow phenomena. This method has been successfully employed for different applications, under-expanded axisymmetric jets [42], multi-jet flows [43], hypersonic shock waves [44], supersonic separated flow [45], and shock waves of a rifle discharge and explosions [12].

The De Laval nozzle (also called the converging-diverging nozzle) is named after its inventor Gustaf de Laval in 19th century. Initially it was designed for steam turbines, it was later widely adapted for use in rocket engines and supersonic wind tunnels [46]. It consist of a converging section, a throat, and a diverging section. The De Laval nozzle's can accelerate subsonic fluid flow to supersonic velocities by carefully designing converging and diverging sections [47]. The nozzle exploits the principles of compressible flow, shock waves, and expansion waves, making it a useful tool for studying high-speed fluid dynamics.

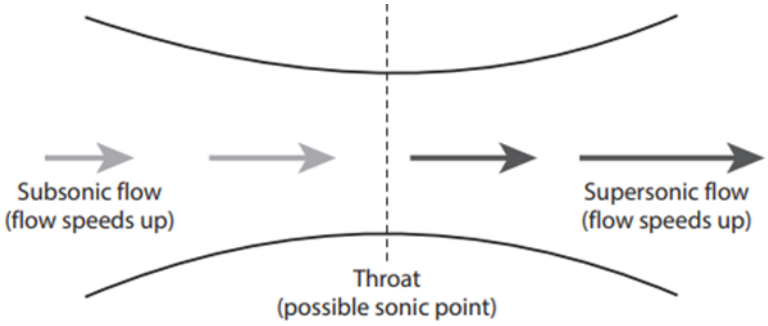

Figure 2.1: Converging-Diverging Nozzle

This research work is influenced by work in the field of schlieren flow visualization technique in Institute of Engineering, Pulchowk Campus [48]. This study presented the design-procedures of the supersonic CD-nozzle along with visualization of the supersonic compressible flow using the optical methods (schlieren, shadowgraph technique).

CHAPTER 3: METHODOLOGY

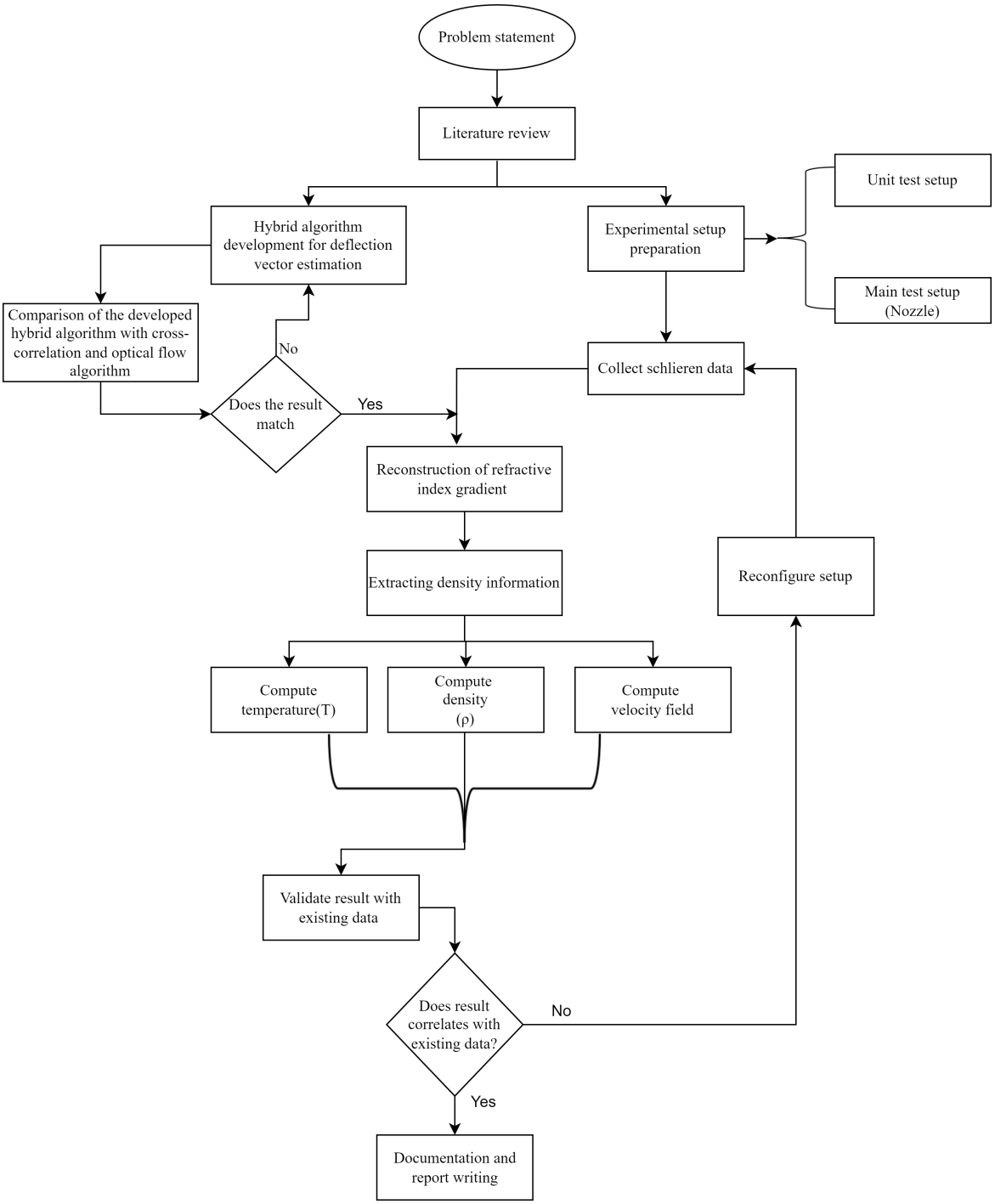

Figure 3.1: Methodology Flow-Chart

3.1 Development of Cross-Correlation Based Image Processing Algorithm

The present study focused on the development of a cross-correlation algorithm using direct cross-correlation. The following section discusses the routines and subroutines of the algorithm developed using MATLAB. The overall procedure of the estimation of the displacement vectors using the cross-correlation algorithm is shown in figure 3.2.

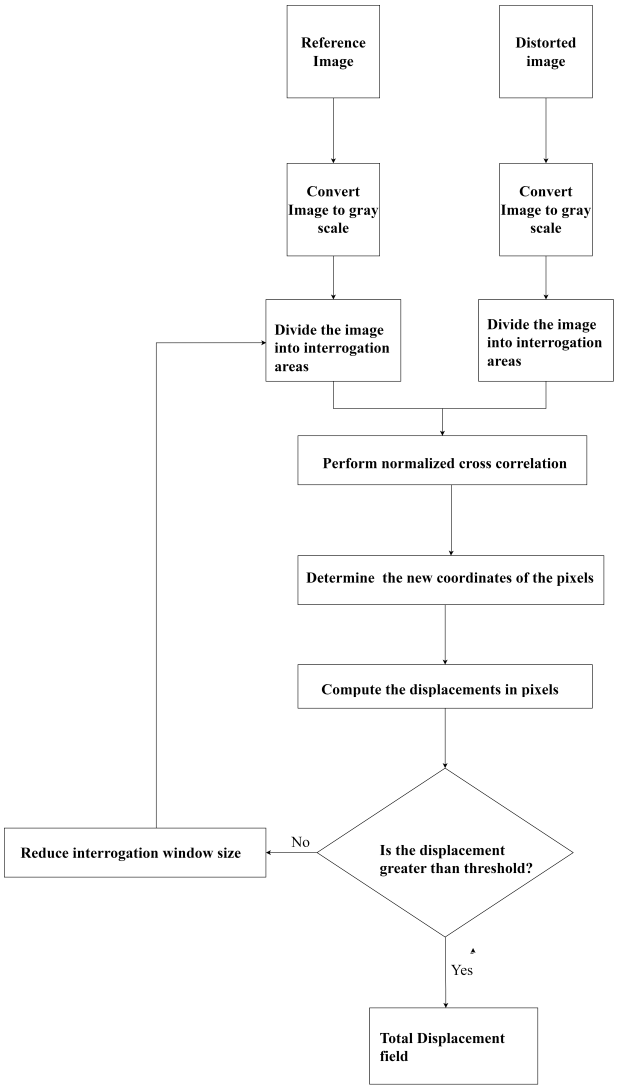

Figure 3.2: Cross-correlation algorithm flow chart

The algorithm loads the two images(reference and distorted images), undergoes image pre-processing (image bit conversion, filtering) and then estimates the displacement vectors. The displacement vector data are then used for the computation of the density field.

3.2 Development of Optical Flow-Based Image Processing Algorithm

The present study focused on the development of Horn and Schunck's optical flow algorithm. The following sections discuss on the major routines and subroutines of the algorithm developed using MATLAB. The basic architecture of the overall image processing code for the estimation of displacement vectors is shown in figure 3.3.
The algorithm works to load a pair of images, sets input parameters relevant to the physics of the flow, undergoes pre-processing of the image data (filtering, correction of illumination), then estimates optical flow. Necessary results are plotted where required. The resulting optical flow estimation has the units in pixels/unit time unless the unit is converted into physical dimensions. For BOS applications, calibration is done typically to obtain the conversion factor. MATLAB functions tabulated as follows in table 3.1. These functions are called in the main script file in MATLAB.

Table 3.1: Optical flow estimation functions list

MATLAB Functions	**Functions**
illumination_correction	Corrects the local and global illumination of image data to incorporate the principle of brightness constancy
filtering	Uses Gaussian filter to remove random noises from images
hs_estimation	Calculates initial optical flow estimation using Horn-Schunck principle
liu_shen_estimator	Calculates optical flow based on the initial estimation provided by hs_estimation
optical flow	Gives estimation of optical flow combining results from both hs_estimation and liu_shen_estimator

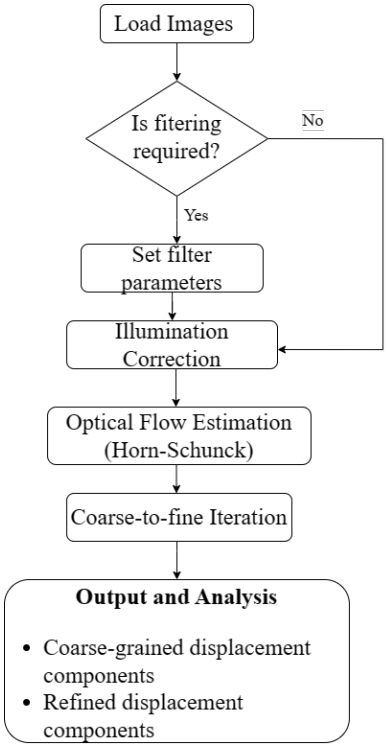

Figure 3.3: Architecture of algorithm developed in MATLAB

3.2.1 Pre-Processing of Images

Loading Data

The image data can be loaded in any format .bmp,.tiff,.png or .jpg. A reference image and a distorted image having the same file format are loaded. The necessary information about the image including bit depth, size and class is displayed in the console. The algorithm developed is designed to work with 8-bit images only. If the loaded images are 12, 14 or 16-bit, they need to be changed to 8-bit images. Further, if the images are RGB channeled, they should be converted to gray-scale.

Correction of Illumination Variations

In the section it has been well established that the underlying assumption of the optical flow estimation is that surface illumination remains fixed from one frame to the next.

However, the brightness constancy cannot be obtained exactly even in well-controlled laboratory conditions. This results in a change in the illumination intensity field in a time interval between two successively acquired images. The following steps are adopted to solve this issue.

1. Developed a subroutine to correct the overall illumination change in the whole image by normalizing both the images
2. Developed a simple scheme to correct local illumination change based on use of Gaussian filter

The input parameter required for the subroutine is provided in the main script as: "size_average". The selection of standard deviation of the filter is crucial to determine the local averaged intensity value for correction. The input size of the filter is in pixels. This subroutine takes both images, a rectangular window for global correction and size of filter as input arguments and returns illumination-corrected images.

```
Pseudocode: correction_illumination
------------------------------------------------------------
-- Step 1: Convert images to double precision

-- Step 2: Initialize modified images

-- Step 3: Adjust overall illumination
           Calculate mean intensity in specified region
           Adjust overall illumination of I2 to match I1

-- Step 4: If size_average is greater than 0,
           Normalize intensity for I2
           Use a spatial averaging filter (filter2)
           else
            No normalization required

-- Step 5: Output corrected images
  return I1, I2
------------------------------------------------------------
```

Figure 3.4: Pseudo code for correction of illumination changes

Filtering

After loading the necessary image data, pre-processing may be sometimes needed in order to remove the random noise. This can be achieved by using the Gaussian filter. This subroutine also requires the standard deviation of the filter and the input is provided in the main script as "mask_size". From the mask size of the filter, the standard deviation of the filter can be calculated as "mask_size" $\times\ 0.6$.
This subroutine takes both images, mask size of the filter, scale factor to down sample the images as input arguments and returns filtered images.

```
Pseudocode: filtering
---------------------------------------------------------------
-- Step 1: Convert images to double precision
   For each pixel in Im1 and Im2:
   Convert pixel intensity to double precision.

-- Step 2: Initialize modified images
  Set I1 as the double precision version of Im1.
  Set I2 as the double precision version of Im2.

-- Step 3: Resize images
  For each image I1 and I2:
  Resize the image using a scaling factor, scale_im.

-- Step 4: Apply Gaussian filter to images
  Set mask_size as the specified size for the Gaussian filter.
  Calculate the standard deviation (std) based on the mask size.

   For each image I1 and I2:
     Create a 2D Gaussian filter, H1 and H2, with the specified mask size and
      standard deviation.
     Apply the Gaussian filter to each image independently.
     Average the results of the two filtered images.

-- Step 5: Output pre-processed images
  Return the pre-processed images I1 and I2.
---------------------------------------------------------------
```

Figure 3.5: Pseudo code for filtering of images

3.2.2 Optical Flow Algorithm

In the section 1.3.2 it was introduced that the energy functional given by equation (1.11) should be minimized to recover the optical flow. Minimizing the energy functional

$E(w) -> min$, following the Euler-Lagrange equation can be obtained.

$$I\nabla\left(\frac{\partial I}{\partial t} + \nabla(Iw) - f\right) + \lambda\nabla^2 w = 0. \tag{3.12}$$

The equation (3.12) can be solved using finite difference method with the Neumann boundary condition $\frac{\partial w}{\partial n} = 0$ on the boundary of the image domain to obtain the finite optical flow $w = (u, v)$.

Horn and Schunck Algorithm

The gradient constraint equation given by equation (1.10) is modeled as follows to give an initial estimation of optical flow. The solution of the model is then used to solve equation (3.12).

The implementation of this algorithm computes the dense motion between two images and optical flow (u, v) are estimated.

In order to compute the spatial and temporal gradients, D1 and F1 matrices are defined as follows.

Spatial Gradient Kernel ($D1$)

The finite difference formulas for spatial derivatives are typically expressed as follows:

$$I_x = \frac{\partial I}{\partial x} \approx \frac{1}{2}\left(I_{i,j+1} - I_{i,j-1}\right)$$

$$I_y = \frac{\partial I}{\partial y} \approx \frac{1}{2}\left(I_{i+1,j} - I_{i-1,j}\right)$$

The matrix $D1$ captures these finite difference coefficients:

$$D1 = \frac{1}{2}\begin{bmatrix} 0 & 0 & 0 \\ 0 & -1 & -1 \\ 0 & 1 & 1 \end{bmatrix}$$

Temporal Gradient Kernel ($F1$)

The finite difference formula for the temporal derivative is expressed as:

$$I_t = \frac{\partial I}{\partial t} \approx \frac{1}{4}\left(I_{i,j+1} + I_{i,j-1} - I_{i-1,j-1} - I_{i+1,j+1}\right)$$

The matrix $F1$ captures these finite difference coefficients:

$$F1 = \frac{1}{4}\begin{bmatrix} 0 & 0 & 0 \\ 0 & 1 & 1 \\ 0 & 1 & 1 \end{bmatrix}$$

Spatial gradients are calculated using convolution with D1, while temporal gradient is calculated using convolution with F1.These gradients represent the rate of change of intensity in x, y and time dimensions. The neighbourhood information is considered. The algorithm refines the flow estimation by solving a linear system of equations based on the optical flow constraints and regularization term.

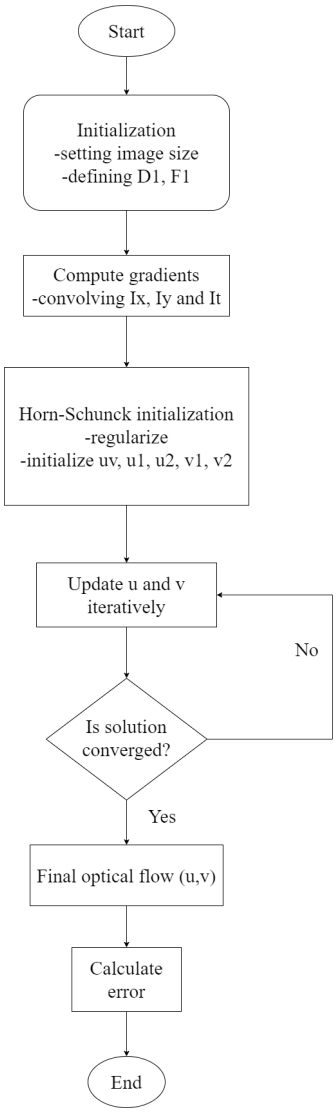

Figure 3.6: Flowchart for Horn-Schunck algorithm

The complete estimation of optical flow occurs only when equation (3.12) is solved. For this, Horn-Schunck estimation is used as an initial approximation for the optical flow. This algorithm refines the flow estimation by considering the physics of image sequence, incorporating a diffusion term f. The regularization parameter λ is set as input at the main script.

3.3 Development of Hybrid Cross-Correlation and Optical Flow Algorithm

As we discussed previously the cross correlation algorithm has lower spatial resolution, providing displacement for every interrogation window. For example, the displacement image generated from the cross-correlation algorithm with IA size $32 \times 32px$ with 50% generates 62×62 displacement vectors for image of size $500 \times 500px$. Sub-pixel interpolation is often incorporated into the cross-correlation algorithm providing more accurate data, however the spatial resolution is still considerably lower than the optical flow algorithm which has high spatial resolution providing displacement for each pixel. Even though optical flow has high spatial resolution, this method becomes less accurate for large displacements.

Need for the high spatial resolution and greater accuracy for all ranges of displacement requires combining both cross-correlation and optical flow algorithm in an iterative manner. Using the cross-correlation algorithm provides a coarse vector fields with low spatial resolution.The optical flow methodology employed in this study adopts a differential approach, proving particularly effective for extracting high-resolution displacement fields characterized by small displacement vectors, typically less than 5 pixels. Hence coarse displacement field from cross-correlation is combined with the results obtained from the optical flow algorithm to get more refined displacement field.

The procedure for implementation of hybrid algorithm is shown in figure 3.7.

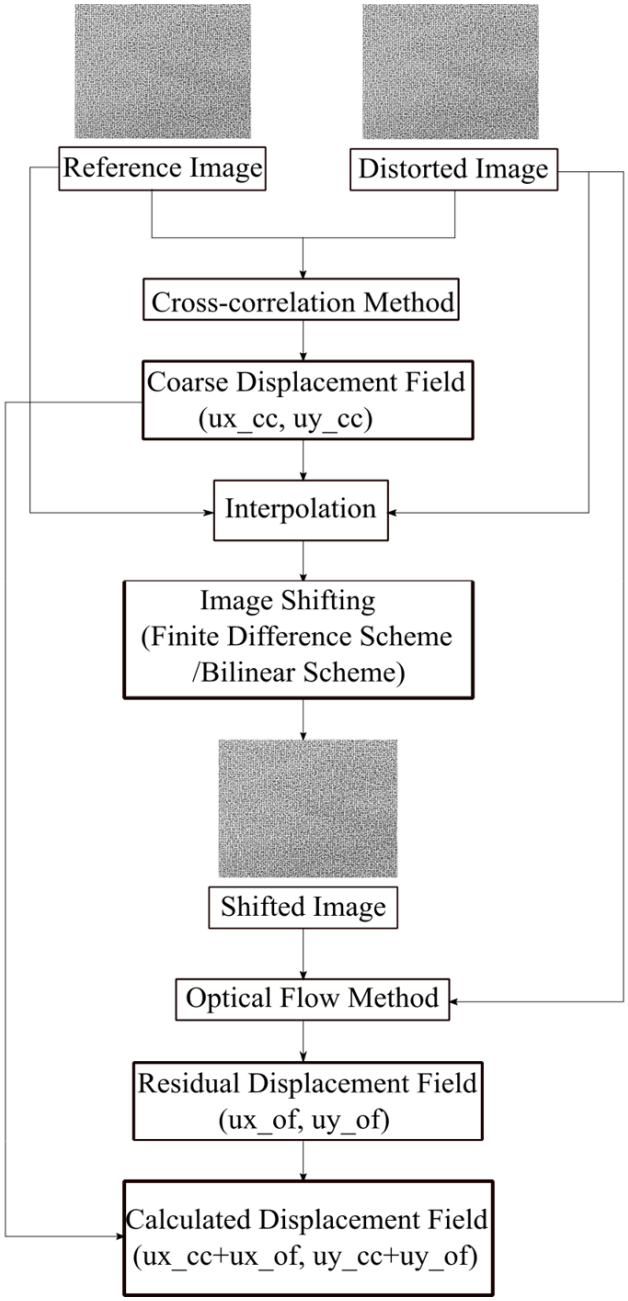

Figure 3.7: Block diagram and working principle of hybrid algorithm

The first set of the displacement (ux_cc, uy_cc) is obtained by applying the cross-correlation algorithm between the reference and distorted image. Since the spatial resolution of the obtained displacement is less than the actual image, cubical interpolation scheme is applied to fill the vector in each pixel. Image shifting scheme is used for image transformation of reference image towards the distorted image. The grey level of every pixel of the new shifted image is found out using finite difference and the bi-linear interpolation technique to include the contribution of the sub-pixel motion. The choice

of shifting reference image to the distorted image or vice versa doesn't affect the result significantly except at the boundaries [40].

Intensity difference compensation and Gaussian filters are applied to the shifted image to reduce the noise associated with image transformation. Optical flow algorithm is applied between the transformed image and the distorted image to obtain the finer displacement vectors. Once the fine displacements are obtained the coarse displacements (obtained from the cross-correlation) and the fine displacements (obtained from the optical flow method) are added to get more accurate displacement values.

Table 3.2: Displacement estimation from hybrid algorithm functions list

MATLAB Functions	**Functions**
cc_main	Undergoes the estimation of coarse displacement field using cross-correlation algorithm
image_shifting_fd	Maps pixel intensity on the input image to form shifted image using finite difference method
image_shifting_bilinear	Maps pixel intensity on the input image to form shifted image using bilinear interpolation scheme
opticalflow_main	Undergoes the estimation of displacement field ($<$1 px) using optical flow algorithm
illumination_correction	Corrects the local and global illumination of image data to incorporate the principle of brightness constancy
filtering	Uses Gaussian filter to remove random noises from images
hs_estimation	Calculates initial optical flow estimation using Horn-Schunck principle
liu_shen_estimator	Calculates optical flow based on the initial estimation provided by hs_estimation
opticalflow	Gives estimation of optical flow combining results from both hs_estimation and liu_shen_estimator
added	Adds displacements from cc_main and opticalflow_main

3.3.1 Interpolation

The cross-correlation method yields calculated vectors based on a cluster of pixels. In contrast, the optical flow method computes a vector for every individual pixel. Hence, necessitating the assignment of vectors to pixels lacking them. This is achieved through bi-cubical interpolation between neighboring points with assigned vectors.

3.3.2 Image Shifting

The image shifting scheme is a two step process. The initial step involves mapping the intensity of each pixel from a specified image onto the shifted image, denoted as I_0, according to a predetermined velocity field measured in pixels per unit time. And the second step is the estimating the contribution of the sub pixel motion [9].
Two different ways have been evaluated for sub pixel evaluation. The first is the finite difference scheme describe by Liu et al [9] and the second is the bilinear interpolation scheme as described by Jambunathan et. al. [39]. In case of the finite difference method the sub-pixel velocity component δu_x and δu_y are estimated. These sub pixel velocity follow the relation

$$\delta I = -\Delta_x(I\delta u_x) - \Delta_y(I\delta u_y) \tag{3.13}$$

which is solved by the forward difference scheme with the spatial difference of δx and δy equals to $1px$. The corrected image intensity finally is going to be

$$I(i,j) = I_0 + \delta I \tag{3.14}$$

where I_0 is the grey scale value obtained at each pixel in the first step.
The second is the bilinear interpolation scheme. In case of the bilinear scheme, which is the extension of the linear function for interpolating function of two variables on a regular grid. In case of the bilinear interpolation the grey scale value at each pixel is given by:

$$I(i,j) = \sum N_i I_i \tag{3.15}$$

Here N_i are the weighting functions. The bilinear interpolation uses the values of the

four neighbouring value to estimate the intensity at the point of interest. The expanded form of the equation 3.15 is given by:

$$\begin{aligned} I(i,j) = (1-\delta u_x)(1-\delta u_y)I(i,j) + (1-\delta u_x)\delta u_y I(i,j+1) + \\ \delta u_x(1-\delta u_y)I(i+1,j) + \delta u_x \delta u_y I(i+1,j+1) \end{aligned} \tag{3.16}$$

3.4 Density Estimation

The following section focuses on the development of program to estimate density using MATLAB. The basic working principle of the program is the reconstruction of the density field based on the Poisson equation given by [49],

$$\frac{\partial^2 n}{\partial x^2} + \frac{\partial^2 n}{\partial y^2} = S(x,y) \tag{3.17}$$

A light beam passing through a speckle pattern will project a image on a camera lens. The rays will refract through angle ϵ. When a medium with different density is set in between the background and the camera, angle ϵ will have an displacement ∇x and ∇y with respect to their original trajectory given by [49]

$$\Delta x = M Z_D \epsilon_x \qquad\qquad \Delta y = M Z_D \epsilon_y \tag{3.18}$$

Optical inhomogeneities refract or bend light rays in proportion to their gradients of refractive index[49].

$$\frac{\partial x^2}{\partial z^2} = \frac{1}{n}\frac{\partial n}{\partial x} \qquad\qquad \frac{\partial y^2}{\partial z^2} = \frac{1}{n}\frac{\partial n}{\partial y} \tag{3.19}$$

Integrating the components of deflection in the x and y directions are

$$\epsilon_x = \frac{\partial x}{\partial z} = \int \frac{1}{n}\frac{\partial n}{\partial x}\partial z \qquad\qquad \epsilon_y = \frac{\partial y}{\partial z} = \int \frac{1}{n}\frac{\partial n}{\partial y}\partial z \tag{3.20}$$

Assuming the change in angle to be small, refractive index n can be considered constant along the width h of the subject,

$$\epsilon_x = \frac{1}{n}\frac{\partial n}{\partial x}h \qquad\qquad \epsilon_y = \frac{1}{n}\frac{\partial n}{\partial y}h \tag{3.21}$$

Substituting this in equation 3.4,

$$\frac{\partial n}{\partial x} = \frac{n_0 \Delta x}{M(Z_D)h} \qquad\qquad \frac{\partial n}{\partial y} = \frac{n_0 \Delta y}{M(Z_D)h} \tag{3.22}$$

which gives required Poisson equation as,

$$\frac{\partial^2 n}{\partial x^2} + \frac{\partial^2 n}{\partial y^2} = \frac{n_0}{M(Z_D)h}\left(\frac{\partial \Delta x(x,y)}{\partial x} + \frac{\partial \Delta y(x,y)}{\partial y}\right) \tag{3.23}$$

Using equation 3.23 density can be estimated. The above Poisson equation can be solved either analytically or numerically. As analytical approach is tedious and time consuming, Numerical approach has been chosen for this current project.

Numerical Approach

There are various ways to solve the Poisson equation such as Finite Element Method (FEM), Finite Volume Method (FVM), Finite Difference method (FDM). FDM has been used in this project for it's simplicity and low computational cost.

Finite Difference Method (FDM)

Laplacian finite difference approximation has been applied on 2D grid with boundary conditions at four of the edge within the rectangular domain.

The partial differential equation of the Poisson equation has been discretized using central difference scheme as,

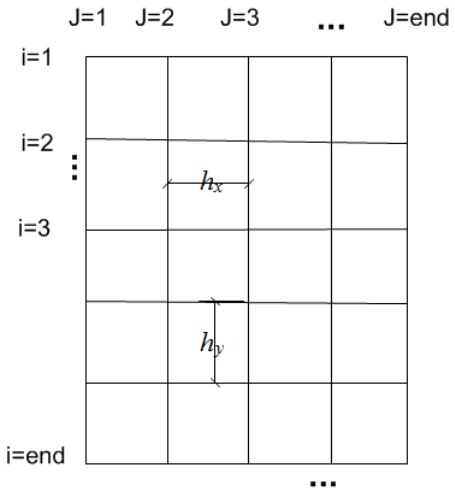

Figure 3.8: Finite difference method grid

$$\left(\frac{U_{i,j-1} - 2U_{i,j} + U_{i,j+1}}{h_x^2} + \frac{U_{i-1,j} - 2U_{i,j} + U_{i+1,j}}{h_y^2}\right) = S(x,y) \tag{3.24}$$

Jacobi Iteration

The Jacobi method is an iterative algorithm for determining the solutions of a diagonally dominant system of linear equations. The process of solving a diagonal element is iterated until it converges. This algorithm is a version of the Jacobi transformation method of matrix diagonalization. The method is named after Carl Gustav Jacob Jacobi [50].

Let $Ax = b$ linear system of n equation

$$A = \begin{bmatrix} a_{11} & a_{12} & \dots & a_{1n} \\ a_{21} & a_{22} & \dots & a_{2n} \\ \vdots & \vdots & \ddots & \vdots \\ a_{n1} & a_{n2} & \dots & a_{nn} \end{bmatrix} \tag{3.25}$$

A and B are known matrices where x is the unknown and can be decomposed into a diagonal component D, a lower part L and an upper part U,

$$A = L+D+U \qquad where, D = \begin{bmatrix} a_{11} & 0 & \dots & 0 \\ 0 & a_{22} & \dots & 0 \\ \vdots & \vdots & \ddots & \vdots \\ 0 & 0 & \dots & a_{nn} \end{bmatrix} \quad and \quad L+U = \begin{bmatrix} 0 & a_{12} & \dots & a_{1n} \\ a_{21} & 0 & \dots & a_{2n} \\ \vdots & \vdots & \ddots & \vdots \\ a_{n1} & a_{n2} & \dots & 0 \end{bmatrix} \tag{3.26}$$

Then solution is obtained as,

$$x^{K+1} = D^{-1}(b - (L+U)x^k) \tag{3.27}$$

In similar fashion the discretized equation of the Poisson equation can be solved. Considering same grid width in x and y direction,

$$h_x = h_y = \Delta x \tag{3.28}$$

$$U_{i,j}^k = -\frac{\Delta x}{4}\left(S_{i,j} - \frac{U_{i-1,j}^{k-1} + U_{i+1,j}^{k-1} + U_{i,j-1}^{k-1} + U_{i,j+1}^{k-1}}{\Delta x^2}\right) \tag{3.29}$$

3.5 Development of Poisson Solver

The present section discusses the development of Poisson solver in MATLAB. The following section discusses the routines and subroutines of the algorithm.

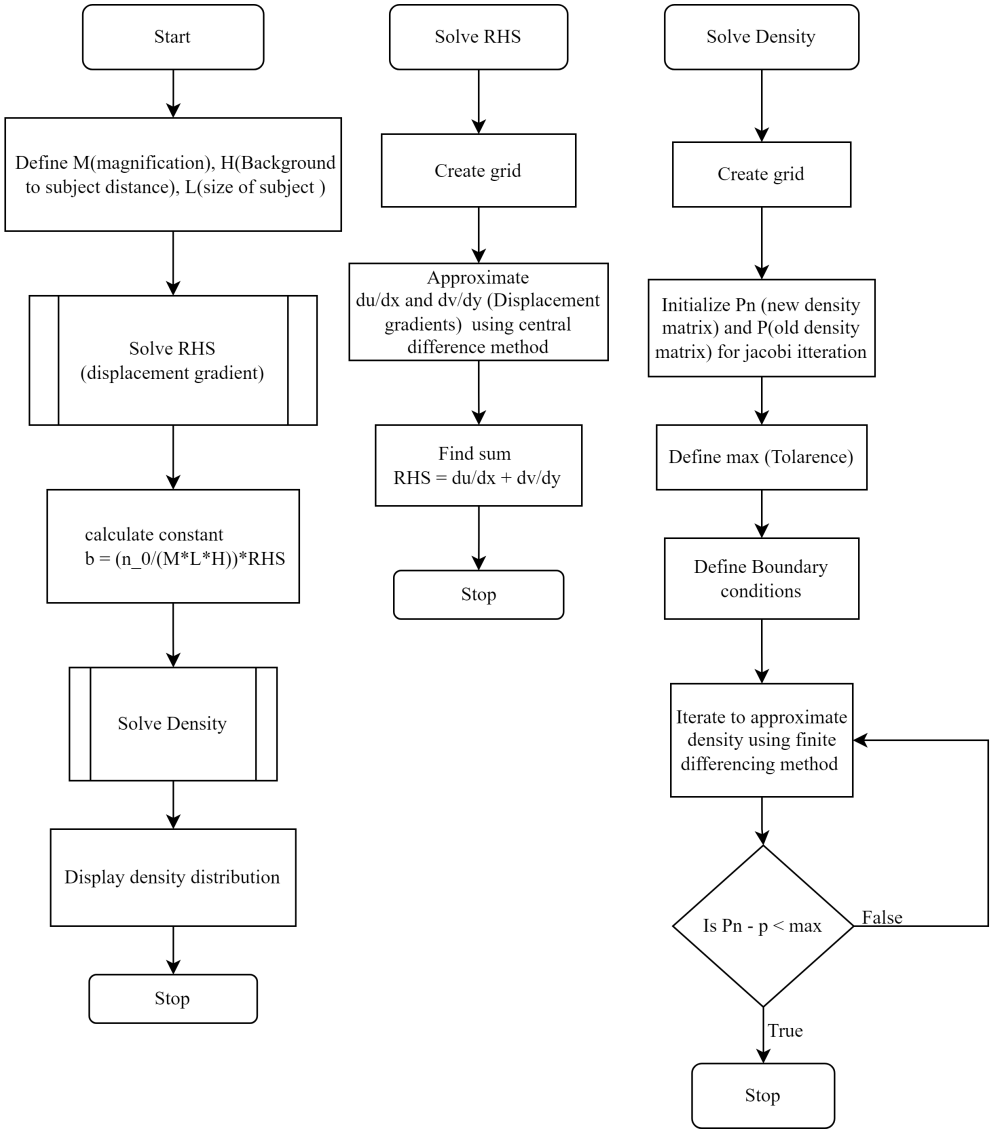

Figure 3.9: Architecture of algorithm developed in MATLAB

For density distribution estimation, displacement matrix obtained from cross-correlation as well as optical flow algorithm can be used. Parameters such as M(magnification), H (distance between background and subject), and L(size of object) need to be defined. The 2 components of RHS of equation 3.23 i.e. displacement gradient and constant are then calculated and multiplied together. Using this required density distribution is obtained which can then be plotted as a contour.

3.5.1 Solve RHS

In equation 3.23, RHS can be decomposed into two parts,constant parameters and displacement gradients.Grid is created and central difference method is applied to approximate $d\Delta x(x,y)/dx$ and $d\Delta y(x,y)/dy$. These two displacement gradients are then added together and hence multiplied by the constant parameters term to find the total RHS of the equation.

$$d\Delta x = \frac{u_{i,j+1} - u_{i,j-1}}{2\Delta x} \qquad d\Delta y = \frac{u_{i+1,j} - u_{i-1,j}}{2\Delta y} \tag{3.30}$$

3.5.2 Solve Density

In order to obtain the required density variation a grid is formulated again. Two new matrices, one for the new density matrix and the other for the old density matrix are then initialized for Jacobi iteration. The maximum tolerance as well as the required boundary conditions are then prescribed. Finally, the finite difference method is used to iterate for the density field.

3.6 Validation of Result

Synthetic image based validation method is adopted in the current study. Long run practice of using standard images to test the effectiveness of the developed algorithms is prevalent when Okamoto et. al in 2000. This method was used to generate standard images for PIV analysis [51].
Recently, Liu et al generated Oseen vortex pair in uniform flow to study the accuracy and to calculate errors in the displacement data [2]. They also compared the data obtained from the cross-correlation and optical flow-based algorithms. In reference to this, the current study also employs the same synthetic images for the Oseen vortex pair in uniform flow. The process of synthetic image generation is explained as follows.

1. Setting up an image: The required image dimensions are defined and the dynamic range of the images are set for example 8-bit image.

2. Generating particles: The number of particles required in the images are set. Whether the distribution of particles are uniformly or pattern-based is decided and the Gaussian intensity distribution is assigned. Finally, particle size and density are set.

3. Temporal evolution: A time step δt is chosen and image deformation algorithm is applied which includes shifting of image.

In regards to the above method, following parameters for synthetic image of Oseen vortex pair are chosen as given in the literature by Liu et. al.

Table 3.3: Parameters taken for the generation of synthetic images

Parameters for Synthetic Images	
Size of image	500x500 pixels
Dynamic range	8-bit
Number of particles	10000
Density of particles	0.04 $1/pixel^2$
Type of intensity distribution of particles	Gaussian
Standard deviation	2 pixels

The following images are to be simulated using the developed algorithms. The pair of images has particles having a mean characteristic image diameter of particles of 4 pixels.

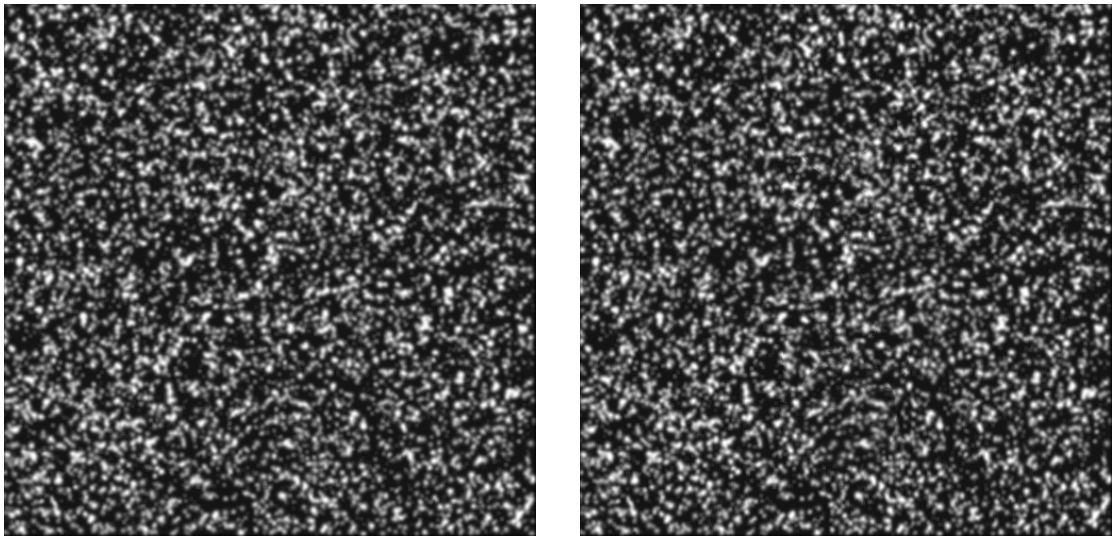

(a) Image without flow imposed (b) Image with flow imposed

Figure 3.10: Pair of Synthetic Images of Oseen Vortex Pair [2]

3.7 Development of Test Setup

3.7.1 Unit Test Setup

To estimate the optimum position of the background, camera and the density gradient requires acquiring multiple data and processing each of those data to identify which set up worked the best. Thus candle was used as the unit test setup on which by hit-and-trial approach the positioning of the optical test bench was determined. The geometrical and optical parameters that was estimated to be the most optimum is tabulated in table 3.4. The images obtained from the unit test setup is shown in figure 3.11.

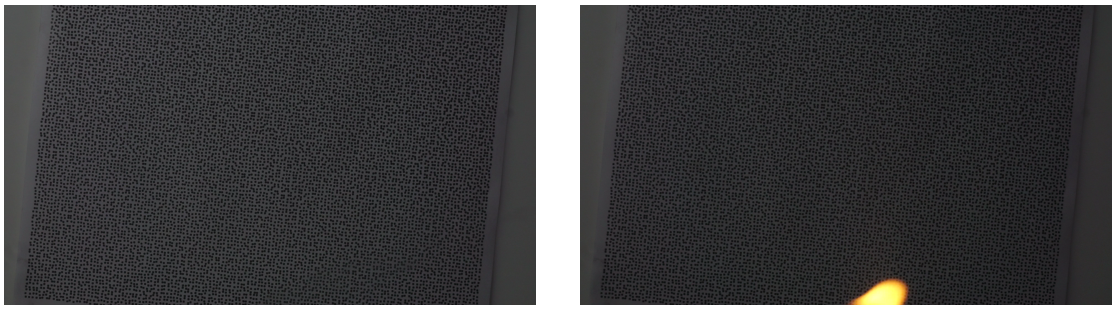

(a) Without background distortion (b) With background distortion

Figure 3.11: Image pair of the unit test setup

Table 3.4: Parameters of test setup considered for candle

Parameters	Distances
Distance between background and test subject (Z_D)	32.5 cm
Distance between test subject and lens(Z_A)	28 cm
Distance between background and lens(Z_B)	60.5 cm
Camera	Sony ZV-E10 Camera
Magnification(M)	1.2

3.7.2 Main Test Setup

The main test setup consisted of the nozzle and pressure chamber. This setup was used for previous used by other researchers [48] [3]. A nozzle is used for this study to generate shock dimaonds from under-expanded jet [3]. The parameters selected for the production of the shock diamonds are described in table 3.5. The setup is shown in the figure 3.12.

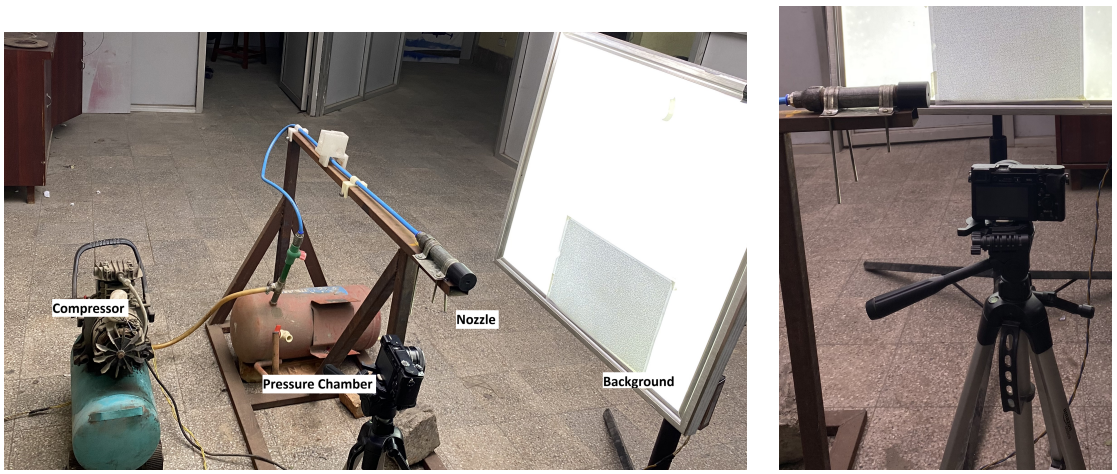

(a) Main test setup (b) Image data acquisition

Figure 3.12: Main test setup key components

Table 3.5: Parameters of test setup considered for under-expanded flow from nozzle

Parameter	**Distances**
Distance between background and density field (Z_D)	28.5 cm
Distance between density field and lens (Z_A)	30 cm
Distance between background and lens (Z_B)	58.5 cm
Camera device	iPhone 11
Magnification	2.7
Frame Rate (fps)	60
Resolution	1920×1080

The 3D printed nozzle as shown in figure 3.13 was used to visualize the under-expanded jet consisting of series of expansion fans and oblique shock waves using Z-type schlieren technique [3]. The same nozzle as shown in figure 3.13 is used in the main test setup.

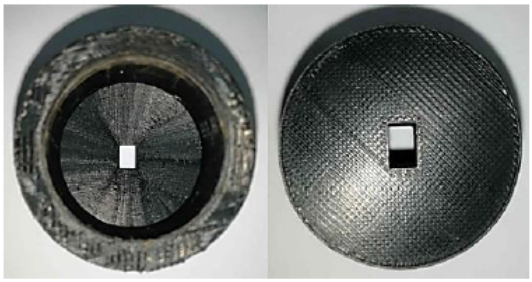

Figure 3.13: 3D printed nozzle adapted from [3]

CHAPTER 4: RESULT AND DISCUSSION

This section explains the results from the Background Oriented Schlieren flow experiments conducted on the test setup and the results obtained from the synthetic images generated through the MATLAB program.
The operation of the algorithm is described in sections 3.1, 3.2, 3.3 and the test setup is described in section 3.7.

4.1 Results

4.1.1 Speckle Pattern Generator

An indispensable part of the setup of the BOS experiment is the background speckle pattern. Though the natural background has been used for the determination of the flow measurements [34], a pattern whose density and size are controlled gives more accurate results. Initially, Gaussian distribution was used for the generation of the background pattern and the image pixel with an array value of less than 0.3 was converted to 0 (white), and pixels with higher values were converted to 1 (black). However, the developed algorithms were unable to pick the displacements of the dots, possibly because of the merging of two or more dots of the speckle pattern.
Then a different approach was taken to develop the speckle pattern. Again, the random numbers were generated but not using the Gaussian distribution. The dots consisted of multiple concentric dots of different shades of gray. This allowed us to more closely control the size of the dots and prevent the overlap between two or more dots. Currently, the images have been taken with black dots on a white background. The white dots on a black background were also tested however owing to the fact that we didn't have the availability of the strong background illumination, we were not able to acquire usable data. The speckle pattern generated using the Gaussian distribution and random number is shown in figure 4.1.

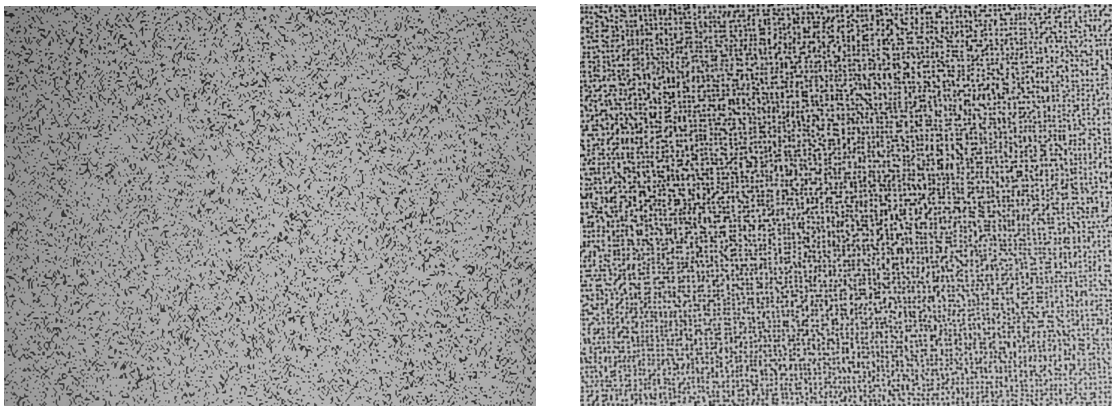

(a) Speckle with Gaussian distribution (b) Speckle with random distribution

Figure 4.1: Pair of generated speckle pattern

4.1.2 Synthetic Image Validation

Displacement Field

The displacement field obtained using the cross-correlation and the optical flow algorithm using the Oseen vortex pair images is described in this section.

Cross-Correlation Algorithm

Using a cross-correlation algorithm the pixel displacements are calculated. Displacement in the x and y direction and the total displacement were computed and the results obtained are described in this section. The methodology of operation of the cross-correlation algorithm is described in section 3.1.

Displacement in x-direction

The result obtained from the cross-correlation algorithm is strongly dependent upon the size of the interrogation area (IA) chosen. For our experiment, we have chosen two interrogation window sizes 16×16 and 32×32. The displacement of the pixels obtained from the cross-correlation algorithm for the IA size of $16 \times 16px$ is shown in figure 4.2. A matrix of 62×62 was obtained containing the displacement values of each IA which was plotted as shown.

The x-displacement for the image pair with the IA of $32 \times 32px$ is shown in figure 4.3. A matrix of 30×30 was obtained and was plotted. Comparing figure 4.2 and figure

4.3 we can see that the use of the small interrogation window produces a more refined displacement field.

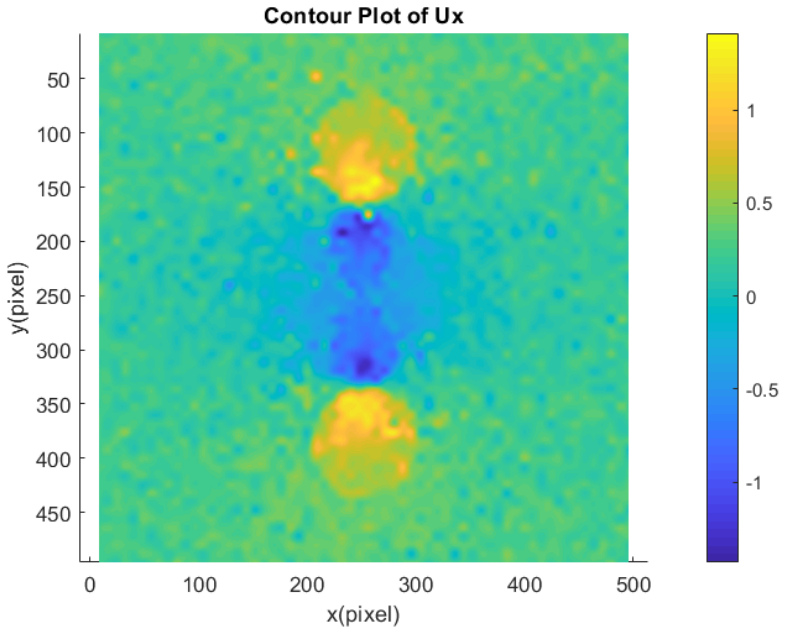

Figure 4.2: Pixel displacement in x-direction for $16 \times 16px$ IA

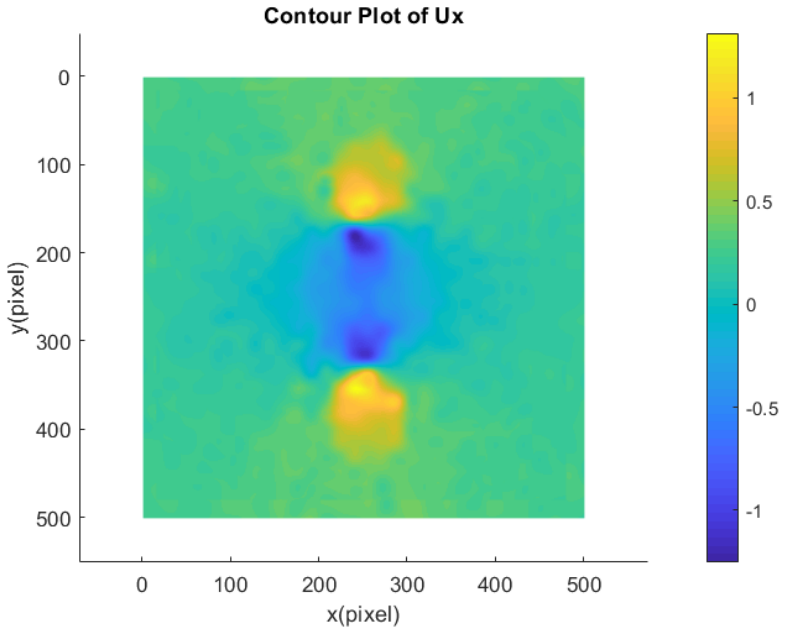

Figure 4.3: Pixel displacement in x-direction for $32 \times 32px$ IA

The minimum displacement obtained in the x-direction was $-1.0962px$ and the maximum pixel displacement obtained was $1.2893px$ for operation with an interrogation

window of $32 \times 32px$. For the operation with the interrogation window size of $32 \times 32px$ we got the maximum and minimum displacement of $1.4022px$ and $-1.4298px$ respectively.

Displacement in y-direction

Again we have chosen two interrogation window size $16 \times 16px$ and $32 \times 32px$. The displacement of the pixels obtained from the cross-correlation algorithm for the IA size of $16 \times 16px$ is shown in figure 4.4. A matrix of 62×62 was obtained containing the displacement values of each IA which was plotted as shown.

The y-displacement for the image pair with the IA of $32 \times 32px$ is shown in figure 4.5. A matrix of 30×30 was obtained and was plotted. Comparing figure 4.4 and figure4.5 we can see that the use of the small interrogation window produces a more refined displacement field.

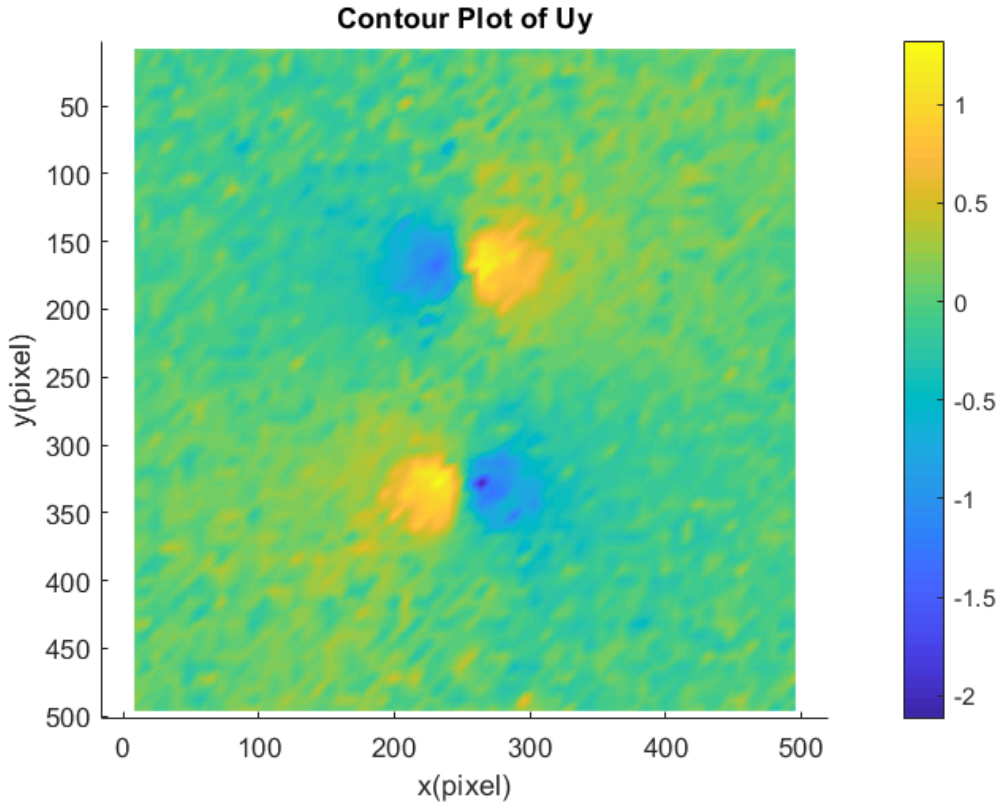

Figure 4.4: Pixel displacement in y direction for $16 \times 16px$ IA

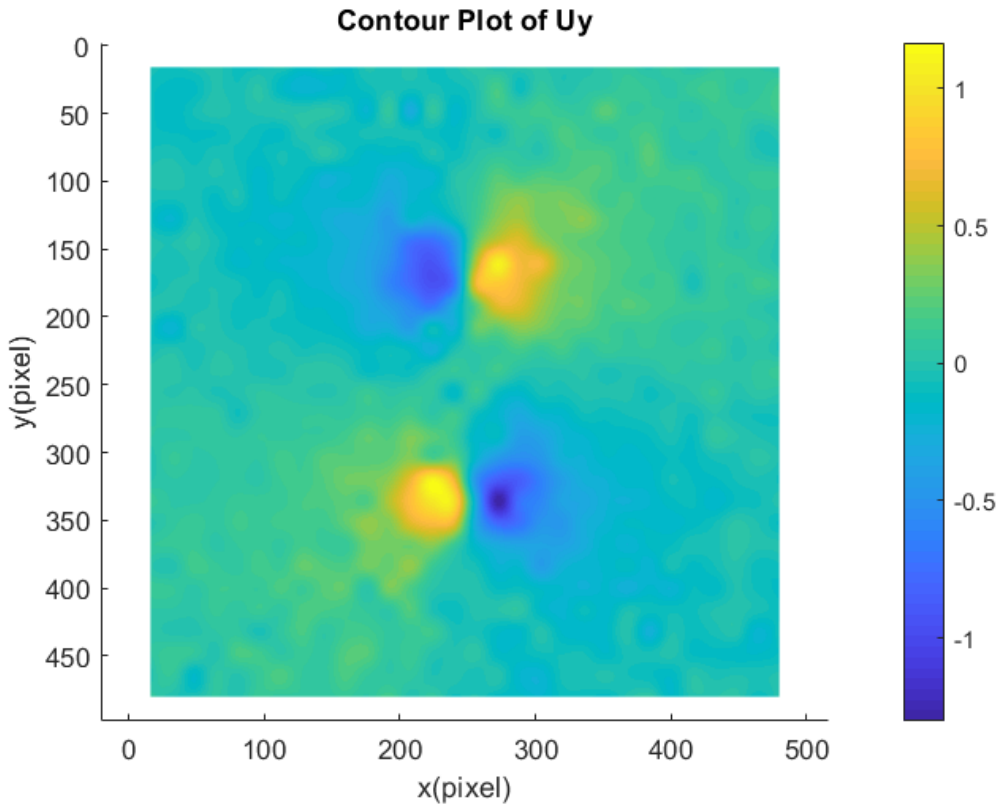

Figure 4.5: Pixel displacement in y direction for $32 \times 32px$ IA

The minimum displacement obtained in y-direction was $-1.295px$ and the maximum pixel displacement obtained was $1.1084px$ for $32 \times 21px$. The minimum displacement obtained in y-direction was $-1.3781px$ and the maximum pixel displacement obtained was $1.3233px$ for $32 \times 32px$. The maximum displacements corresponded to the region of the vortex pair as expected.

Total displacement

Again we have chosen two interrogation window size $16 \times 16px$ and $32 \times 32px$. The displacement of the pixels obtained from the cross-correlation algorithm for the IA size of $16 \times 16px$ is shown in figure 4.6. A matrix of 62×62 was obtained containing the displacement values of each IA which was plotted as shown.

The total displacement for the image pair with the IA of $32 \times 32px$ is shown in figure 4.7. A matrix of 30×30 was obtained and was plotted. Comparing figure 4.6 and figure 4.7 we can see that the use of the small interrogation window produces a more refined displacement field.

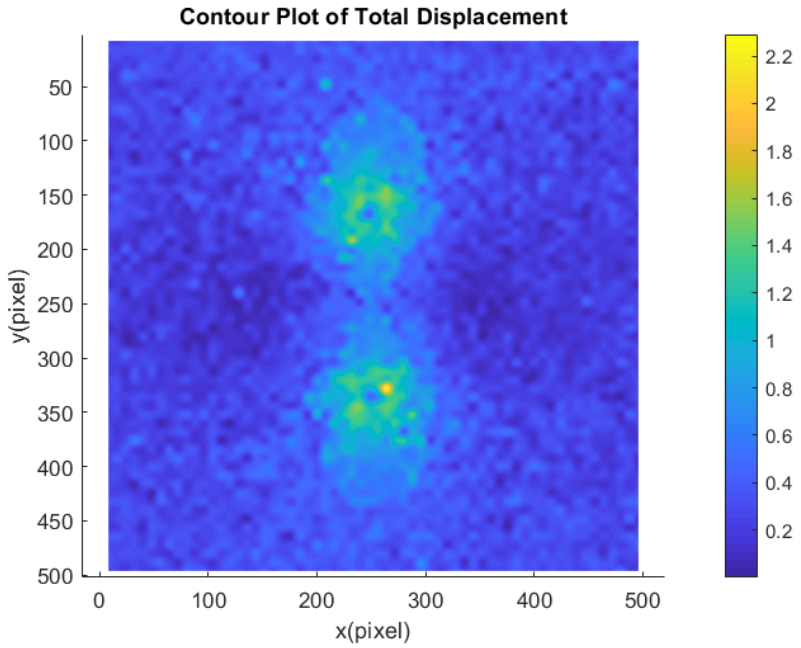

Figure 4.6: Total Pixel displacement for $16 \times 16px$ IA

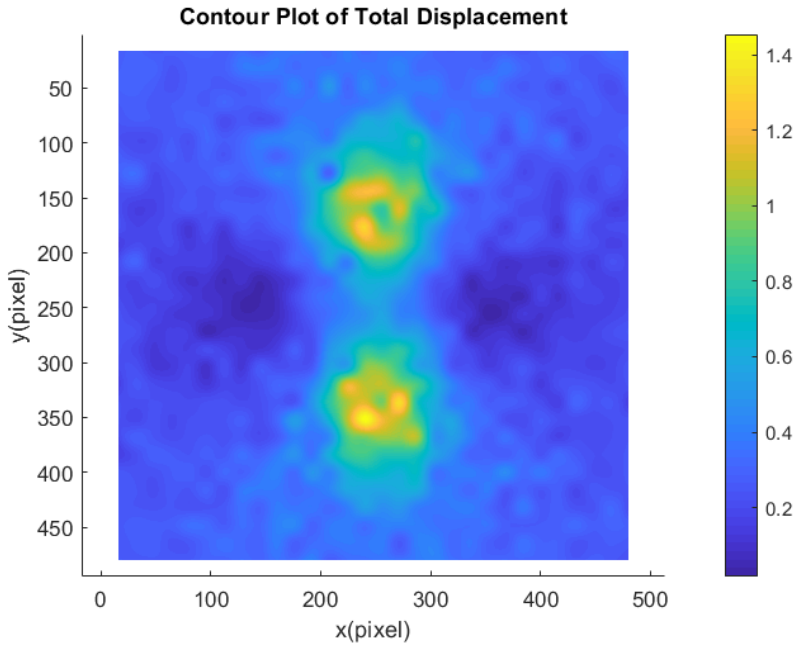

Figure 4.7: Total Pixel displacement for $32 \times 32px$ IA

The minimum total displacement was $0.0211px$ and the maximum total pixel displacement obtained was $1.4513px$ for $32 \times 32px$ IA. The minimum total displacement obtained was $0.01px$ and the maximum total pixel displacement obtained was $1.6358px$

for $16 \times 16px$. The maximum displacements corresponded to the region of the vortex pair as expected.

Vector Plot

The quiver plot of the vector lines indicating the direction of the movement of the pixels for $16 \times 16px$ and $32 \times 32px$ is shown in figure 4.8a and figure 4.8b respectively. The direction of the arrows indicates the displacement of the pixels from the original position as seen in the reference image to the distorted position due to the Oseen vortex. As expected the direction of the vectors aligned perfectly with the synthetic Oseen vortex superimposed on the original image.

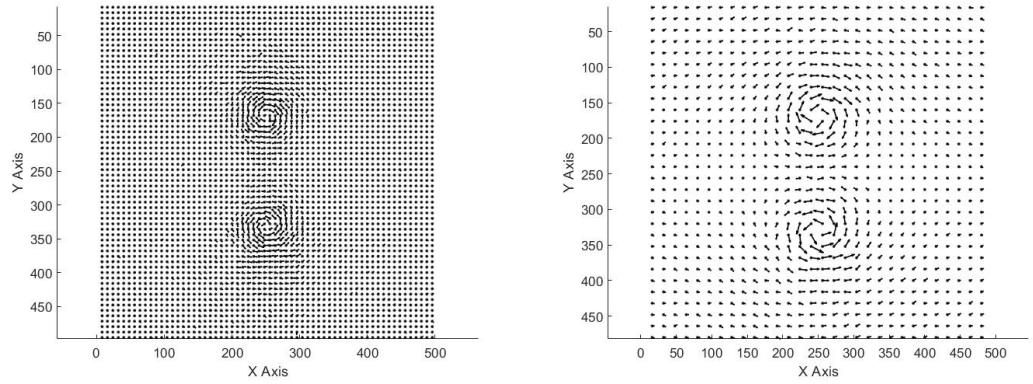

(a) Vector showing direction of pixel movement for $16 \times 16px$ IA

(b) Vector showing direction of pixel movement for $32 \times 32px$ IA

Figure 4.8: Vector plots

Optical Flow Algorithm

Using the Horn and Schunck-based optical flow algorithm, the pixel displacements in the synthetic images are calculated. Displacement in the x, and y axes and the total resultant displacement were computed and the results obtained are described in this section. The methodology of operation of the optical flow algorithm is described in section 3.2.

Displacement in x-direction

The displacement of the pixels obtained from the developed optical flow algorithm is

shown in figure 4.9. The resulting displacement vector has a size of 500x500 as expected for the optical flow algorithm. This is because the optical flow algorithm generates one vector per pixel.

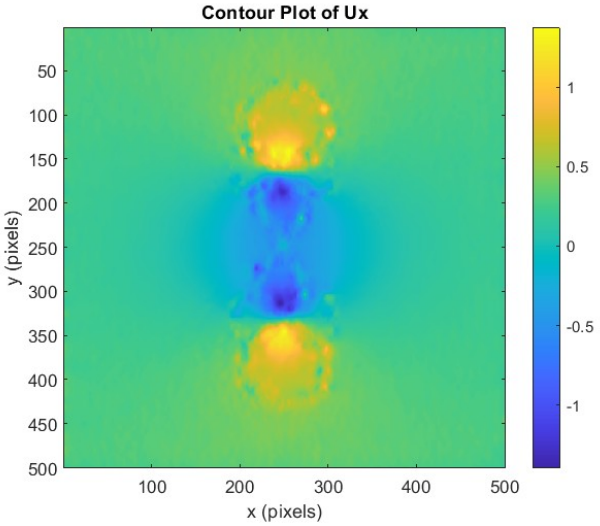

Figure 4.9: Pixel displacement in x direction

Displacement in y-direction

The displacement of the pixels in the y direction obtained from the optical flow algorithm is shown in figure 4.10. Similar to displacement vectors in the x-direction, the displacement vector in the y-direction also has a size of 500x500 as expected.

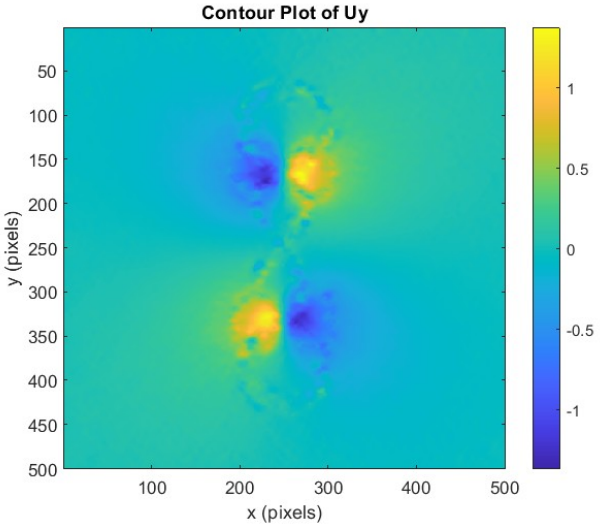

Figure 4.10: Pixel displacement in y direction

Total displacement

The total displacement of the pixels obtained from the optical flow algorithm is shown in figure 4.11. The contour plot is obtained after determining the resultant displacement vectors.

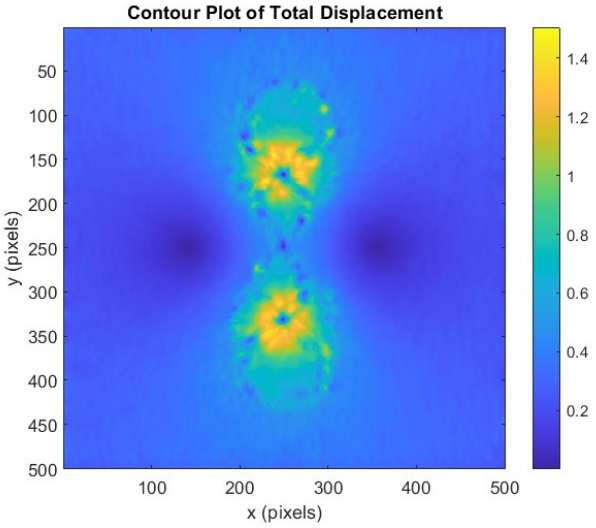

Figure 4.11: Total pixels displacement

Vector Plot

The quiver plot of the vector lines indicating the direction of the movement of the pixels is shown in figure 4.12. The direction of the arrows indicates the displacement of the pixels from the original position as seen in the reference image to the distorted position due to the Oseen vortex. As expected the direction of the vectors aligned perfectly with the synthetic Oseen vortex superimposed on the original image. Also, a comparison of the velocity field before and after refinement is shown in figure 4.12

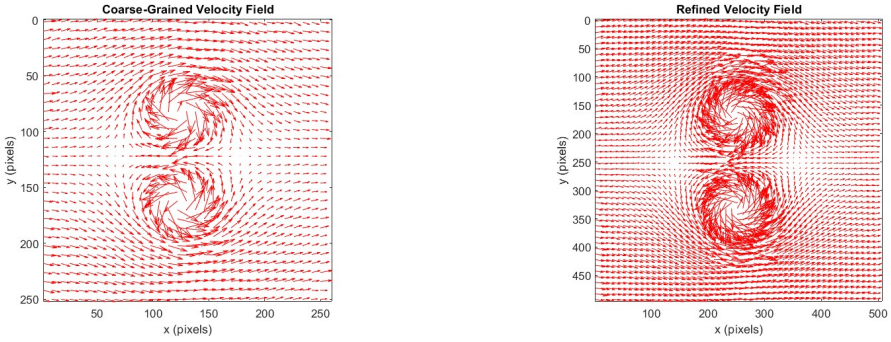

(a) Coarse velocity field

(b) Refined velocity field

Figure 4.12: Comparison of velocity vector plots

Hybrid Algorithm

Using the Hybrid algorithm, the pixel displacements in the synthetic images are calculated. Displacement in the x, and y axes and the total resultant displacement were computed and the results obtained are described in this section. The methodology of operation of the hybrid algorithm is described in section 3.3.

Displacement in x-direction

The displacement of the pixels obtained from the developed hybrid algorithm is shown in figure 4.13. The resulting displacement vector has a size of 500x500.

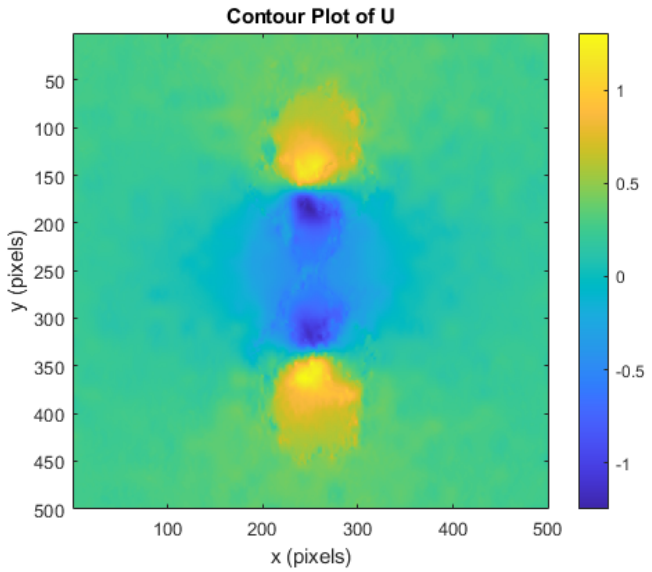

Figure 4.13: Pixel displacement in x direction

The minimum displacement obtained in the x-direction was $-1.2493px$ and the maximum pixel displacement obtained was $1.3084px$.

Displacement in y-direction

The displacement of the pixels in the y direction obtained from the hybrid algorithm is shown in figure 4.14. Similar to displacement vectors in the x-direction, the displacement vector in the y-direction also has a size of 500x500 as expected.

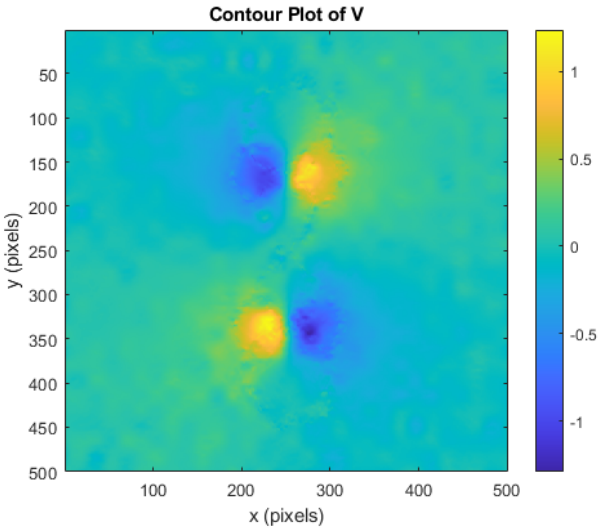

Figure 4.14: Pixel displacement in y direction

The minimum displacement obtained in the y-direction was $-1.2901px$ and the maximum pixel displacement obtained was $1.2375px$.

Total displacement

The total displacement of the pixels obtained from the hybrid algorithm is shown in figure 4.15. The contour plot is obtained after determining the resultant displacement vectors.

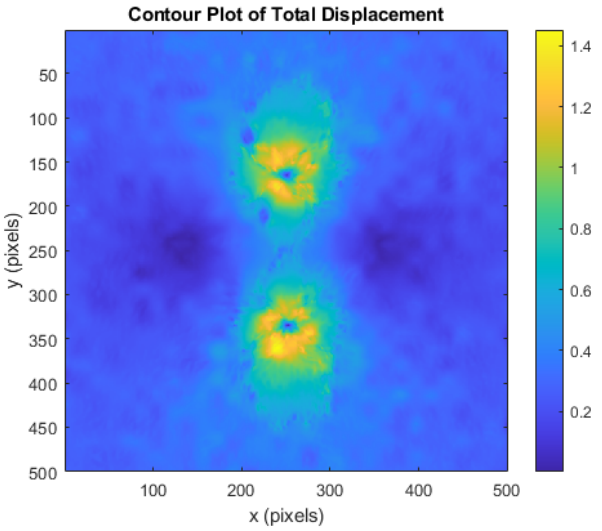

Figure 4.15: Total pixels displacement

The minimum displacement obtained was $0.0016px$ and the maximum pixel displace-

ment obtained was $1.4526px$.

Vector Plot

The quiver plot of the vector lines indicating the direction of the movement of the pixels is shown in figure 4.16. The direction of the arrows indicates the displacement of the pixels from the original position as seen in the reference image to the distorted position due to the Oseen vortex. As expected the direction of the vectors aligned perfectly with the synthetic Oseen vortex superimposed on the original image.

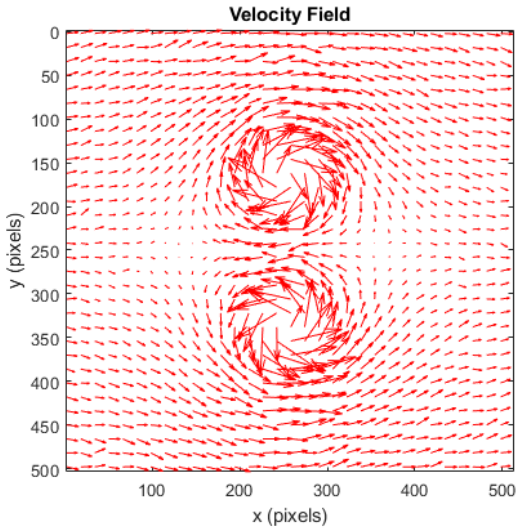

Figure 4.16: Vectors representing displacement

Comparison of displacements obtained from cross-correlation and optical flow algorithm

Table 4.1: Resulting displacement vectors using cross-correlation algorithm

Interrogation Area	Output Displacement Field
16 x 16 pixels (50% overlap)	62 x62 pixels
32 x 32 pixels (50% overlap)	30 x30 pixels

Table 4.2: Resulting displacement vectors using optical flow algorithm

Input Images	Output Displacement Field
500 x 500 pixels	500 x500 pixels

4.1.3 Unit Test Setup

For the unit test setup, hot plumes from the candle were studied. The positioning of the test setup is described in section 3.7. The results obtained from the image taken are described in this section.

Calibration Method

The results from the displacement were obtained in terms of pixels. However, in order to have proper analysis, the pixel results need to be converted to the real physical dimensions of length such as meters. The calibration of the unit test setup after having determined the optimum geometrical and optical parameters in table 4.3.
The image as shown in figure 4.17 is used for the calibration.

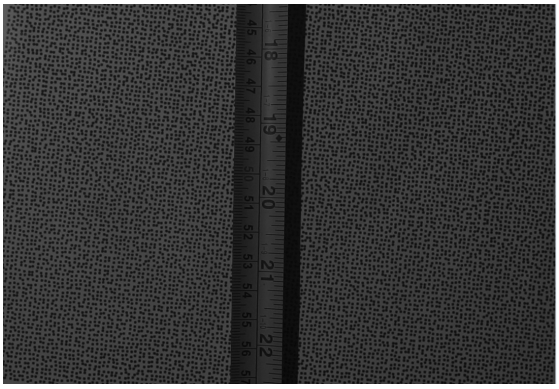

Figure 4.17: Calibration image for unit test setup

The result of calibration is shown in table 4.3.

Table 4.3: Calibration parameters for unit test setup

$1\ px = 0.00012$m

Results from Cross-Correlation Algorithm

The results obtained for unit test setup using a cross-correlation algorithm are described in this section.

Displacement in x-direction

The displacement of the pixels in the x-direction using the cross-correlation algorithm is shown in figure 4.18.

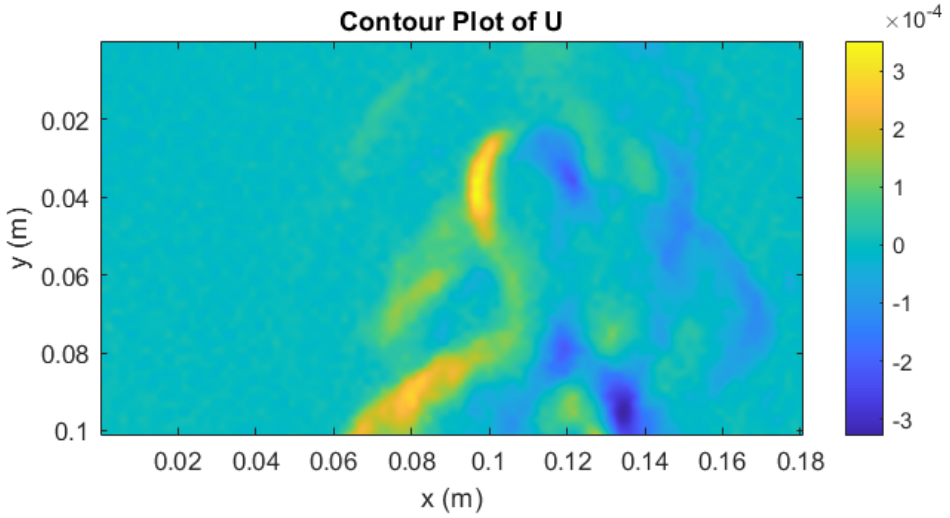

Figure 4.18: Pixel displacement in x-direction for candle plume

The maximum pixel displacement in the x direction was 3.51×10^{-4}m and minimum pixel displacement was -3.28×10^{-4}m.

Displacement in y-direction

The displacement of the pixels in the y-direction using the cross-correlation algorithm is shown in figure 4.19.

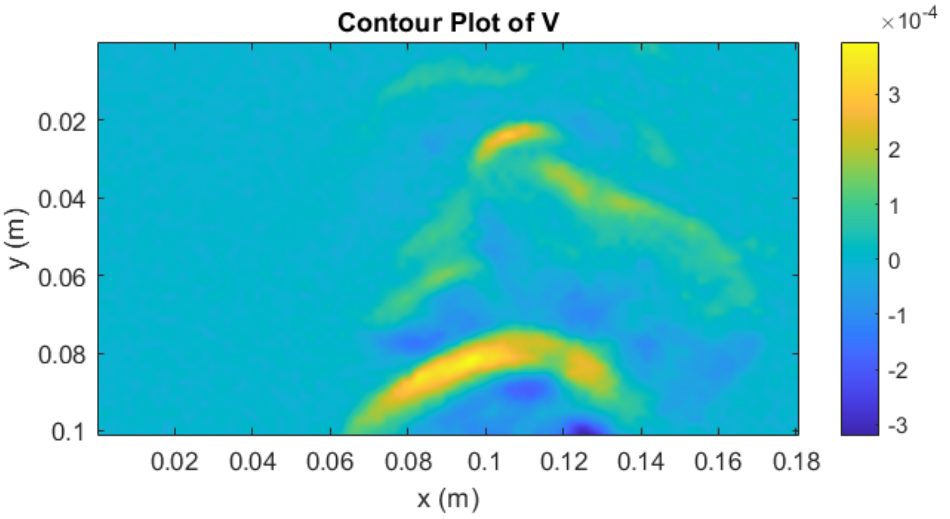

Figure 4.19: Pixel displacement in the y direction for candle plume

The maximum pixel displacement in the y direction was 3.95×10^{-4}m and minimum pixel displacement was -3.2064×10^{-4}m.

Total displacement

The total displacement of the pixels using the cross-correlation algorithm is shown in figure 4.20.

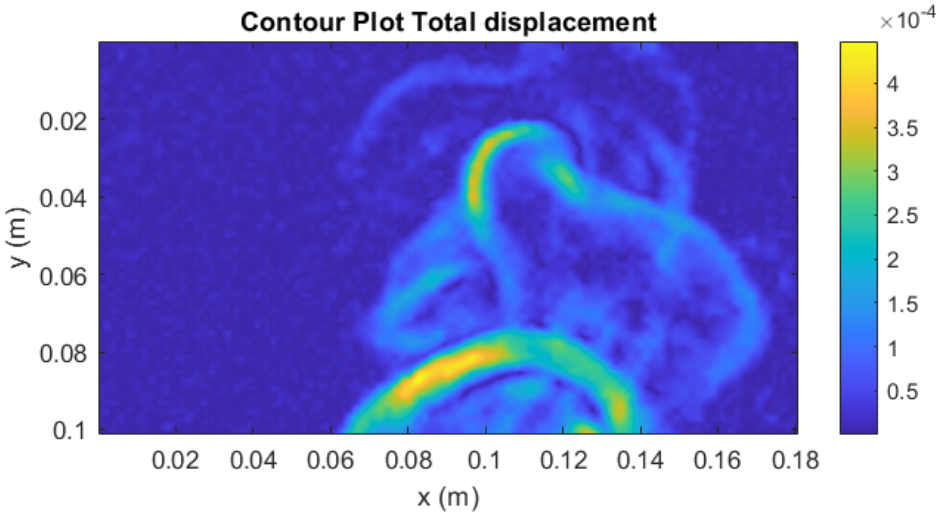

Figure 4.20: Total pixel displacement for candle plume

The maximum pixel displacement was 4.47×10^{-4}m and minimum pixel displacement was 1.25×10^{-8}m.

Results from Optical Flow Algorithm

The results obtained for unit test setup using the optical flow algorithm are described in this section.

Displacement in x-direction

The displacement of the pixels in the x-direction using the optical flow algorithm is shown in figure 4.21.

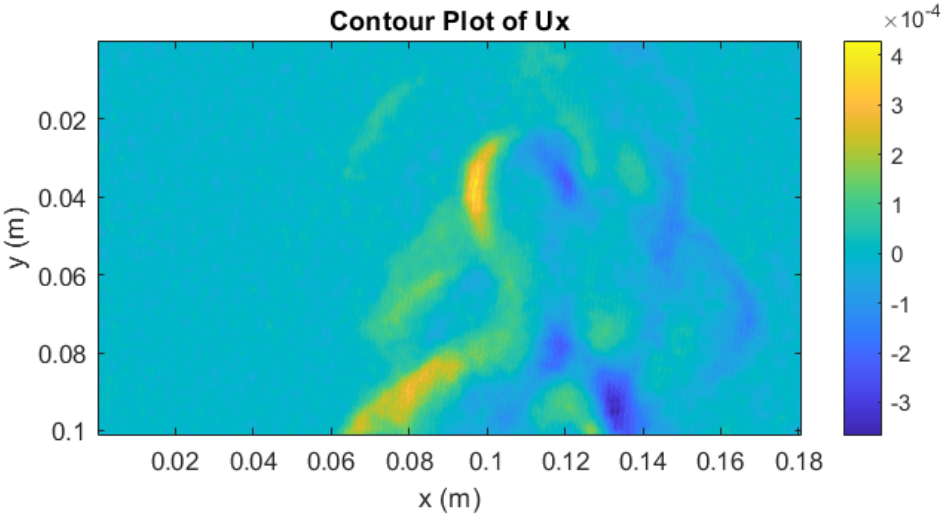

Figure 4.21: Pixel displacement in x-direction for candle plume

The maximum pixel displacement in the x direction was 4.2967×10^{-4}m and minimum pixel displacement was -3.67×10^{-4}m.

Displacement in y-direction

The displacement of the pixels in the y-direction using the optical flow algorithm is shown in figure 4.22.

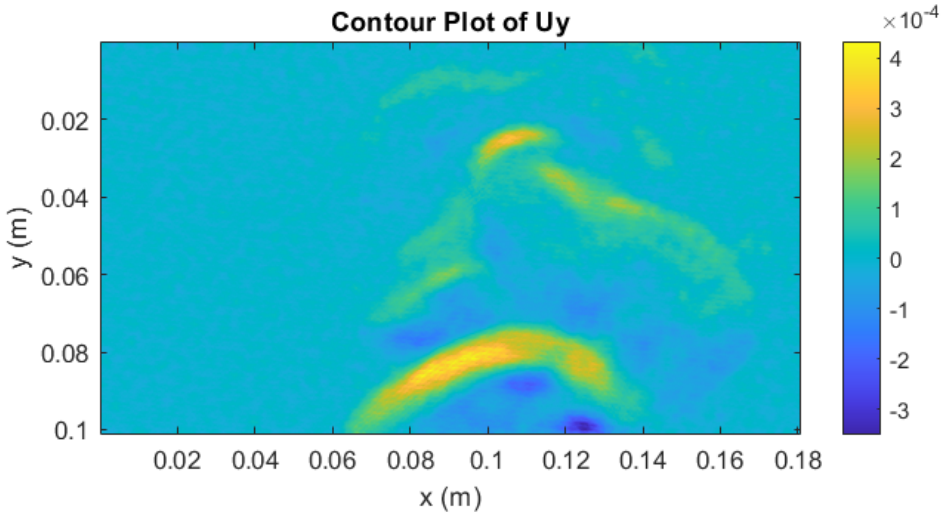

Figure 4.22: Pixel displacement in the y direction for candle plume

The maximum pixel displacement in the y direction was 4.329×10^{-4}m and minimum pixel displacement was -3.5×10^{-4}m.

Total displacement

The total displacement of the pixels using the optical flow algorithm is shown in figure 4.23.

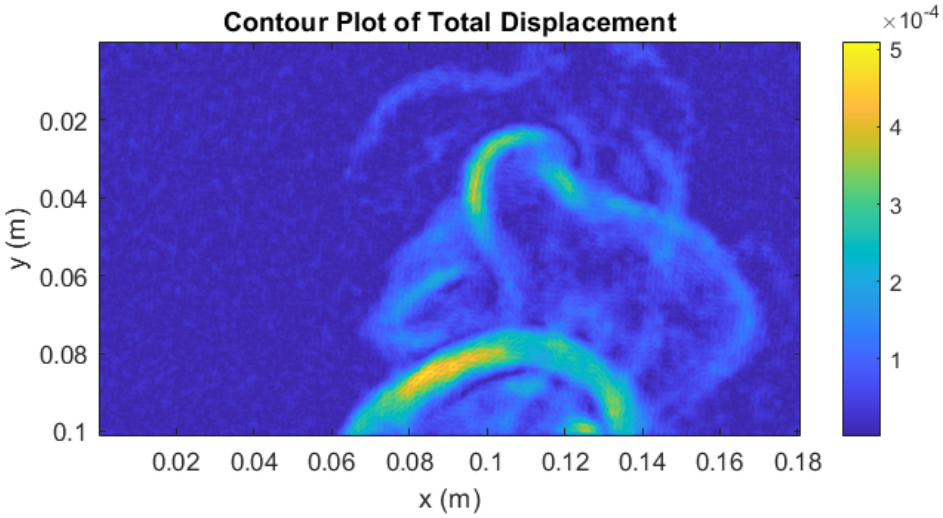

Figure 4.23: Total pixel displacement for candle plume

The maximum pixel displacement was 5.1030×10^{-4}m and minimum pixel displacement was 1.23×10^{-8}m.

Results from Hybrid Algorithm

The results obtained for unit test setup using the hybrid algorithm are described in this section.

Displacement in x-direction

The displacement of the pixels in the x-direction using the hybrid algorithm is shown in figure 4.24.

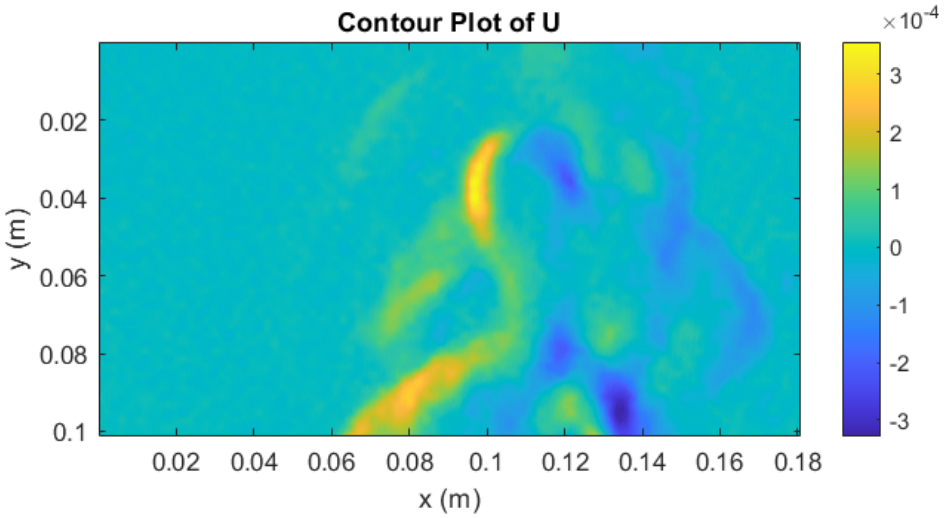

Figure 4.24: Pixel displacement in x-direction for candle plume

The maximum pixel displacement in the x direction was 3.56×10^{-4}m and minimum pixel displacement was -3.28×10^{-4}m.

Displacement in y-direction

The displacement of the pixels in the y-direction using the hybrid algorithm is shown in figure 4.25.

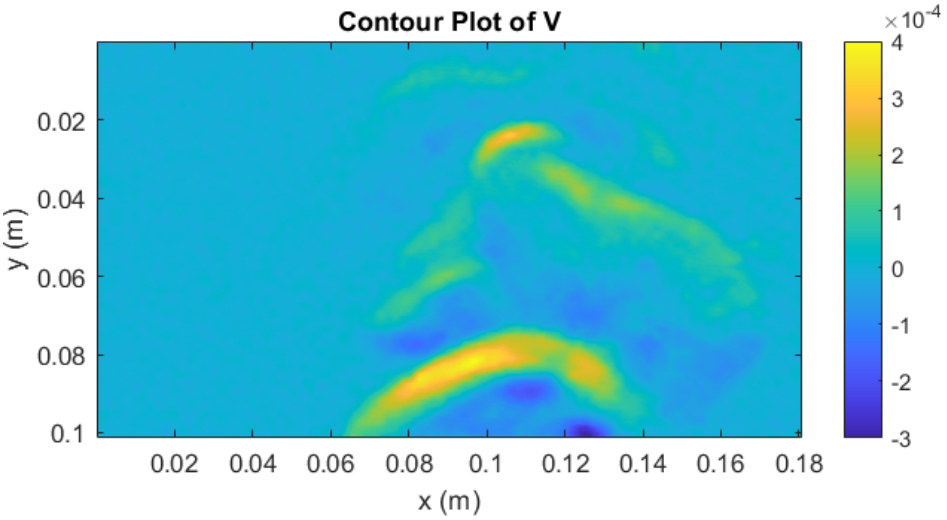

Figure 4.25: Pixel displacement in the y direction for candle plume

The maximum pixel displacement in the y direction was 4.0035×10^{-4}m and minimum pixel displacement was -3.0064×10^{-4}m.

Total displacement

The total displacement of the pixels using the hybrid algorithm is shown in figure 4.26.

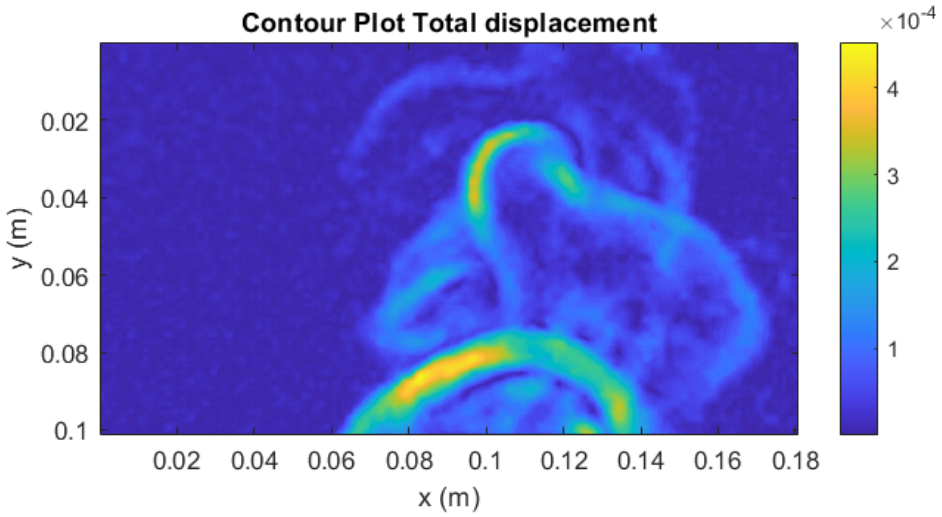

Figure 4.26: Total pixel displacement for candle plume

The maximum pixel displacement was 4.477×10^{-4}m and minimum pixel displacement was 1.2553×10^{-8}m.

4.1.4 Main Test Setup

The main test setup was a nozzle with a pressure chamber. This setup was built by [48]. In the current study, this same setup is used with different nozzle developed by [3], to study the under-expanded nozzle flow. The ambient conditions while performing the experiment were 1 atm pressure and the ambient temperature was 16^0C. The reservoir pressure was 7 atm. The results obtained from the post-processing of the main setup images are described in this section.

Calibration Method

The results from the displacement were obtained in terms of pixels. However, in order to have proper analysis, the pixel results need to be converted to the real physical dimensions of length such as meters. The calibration of the setup after having determined

the optimum geometrical and optical parameters in table 3.5.

The image as shown in figure 4.27 is used for the calibration.

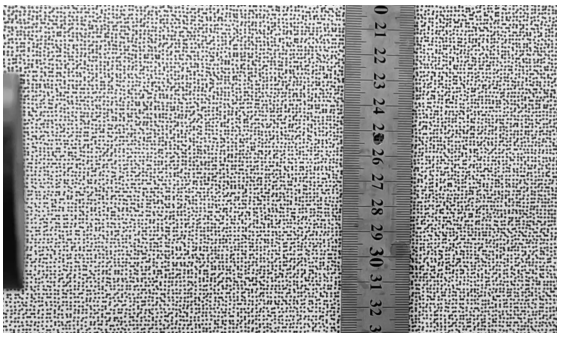

Figure 4.27: Calibration image for visualization of shock diamond

The result of calibration is shown in table 4.4.

Table 4.4: Calibration parameters for main test setup

1 px = 0.00013 m
1 $px/frame$ = 0.0075 m/s

Results from Cross-Correlation Algorithm

Displacement in x-direction

The pixel displacement in x direction using the cross-correlation algorithm is shown in the figure 4.28.

The size of the IA was $16 \times 16px$ The maximum pixel displacement in the x-direction was 1.2361×10^{-4}m while the minimum pixel displacement was -2.9290×10^{-4}m.

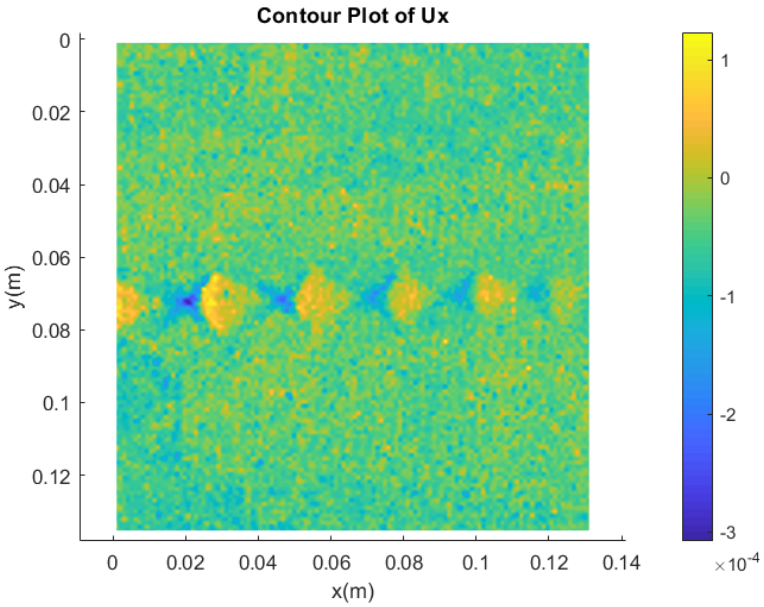

Figure 4.28: Pixel displacement in x-direction for nozzle flow with $16 \times 16px$ IA

Displacement in y-direction

The pixel displacement in the y direction using the cross-correlation algorithm is shown in figure 4.29.

The size of the IA was $16 \times 16px$ The maximum pixel displacement in the y-direction was 1.2512×10^{-4}m while the minimum pixel displacement was -3.1166×10^{-4}m.

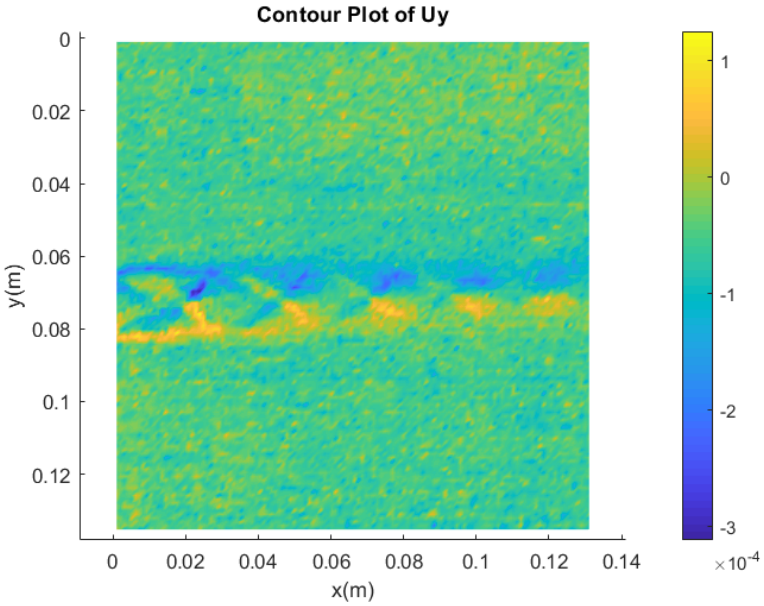

Figure 4.29: Pixel displacement in y-direction for nozzle flow with $16 \times 16px$ IA

Total displacement

The total pixel displacement using the cross-correlation algorithm is shown in figure 4.30.

The size of the IA was $16 \times 16px$. The maximum pixel displacement was 3.7565×10^{-4} m while the minimum pixel displacement was $1.3719 \times 10{-}6$m.

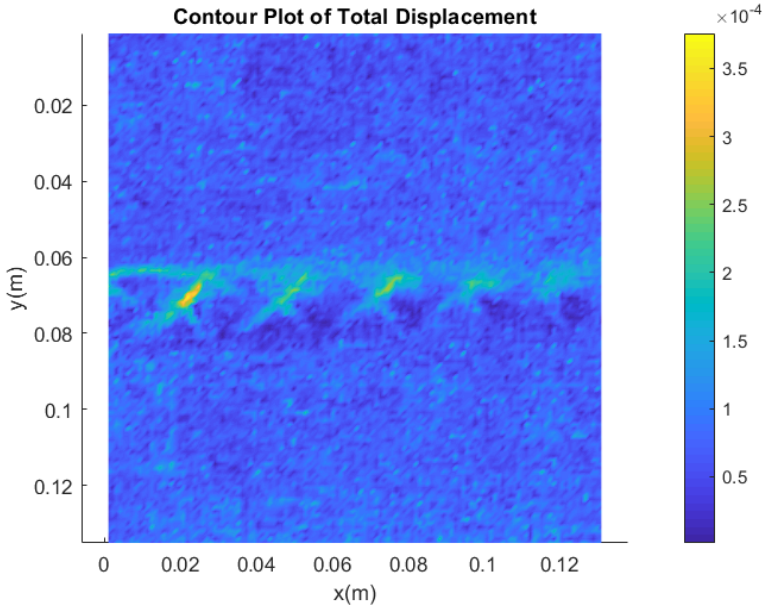

Figure 4.30: Total pixel displacement for nozzle flow for $16 \times 16px$ IA

Results from Optical Flow Algorithm

Displacement in x-direction

The pixel displacement in the x direction using the optical flow algorithm is shown in figure 4.31.

The size of the output displacement field is 1044x1014 which is same as the size of the input images. The maximum pixel displacement in the x-direction was $4.91 \times 10^{-4}m$ while the minimum pixel displacement was $-4.33 \times 10^{-4}m$.

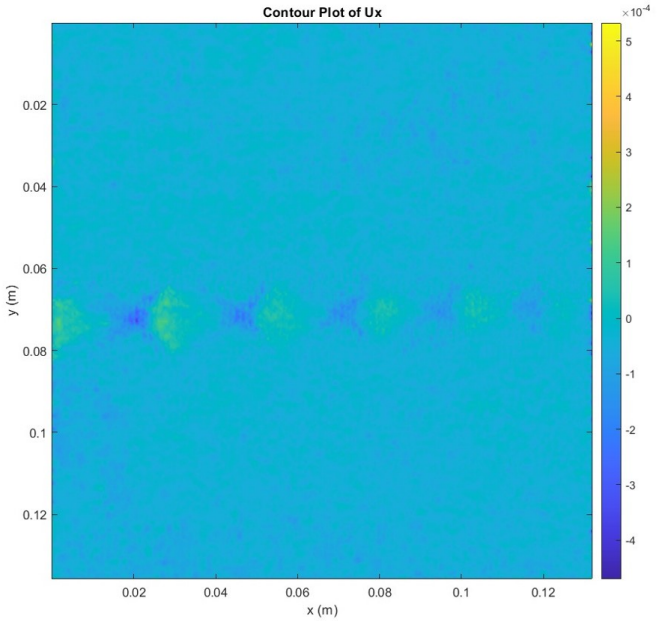

Figure 4.31: Pixel displacement in x-direction for nozzle flow using optical flow

Displacement in y-direction

The pixel displacement in the y direction using the optical flow algorithm is shown in the figure 4.32. The maximum pixel displacement in the y-direction was $2.58 \times 10^{-4}m$ while the minimum pixel displacement was $-4.106 \times 10^{-4}m$.

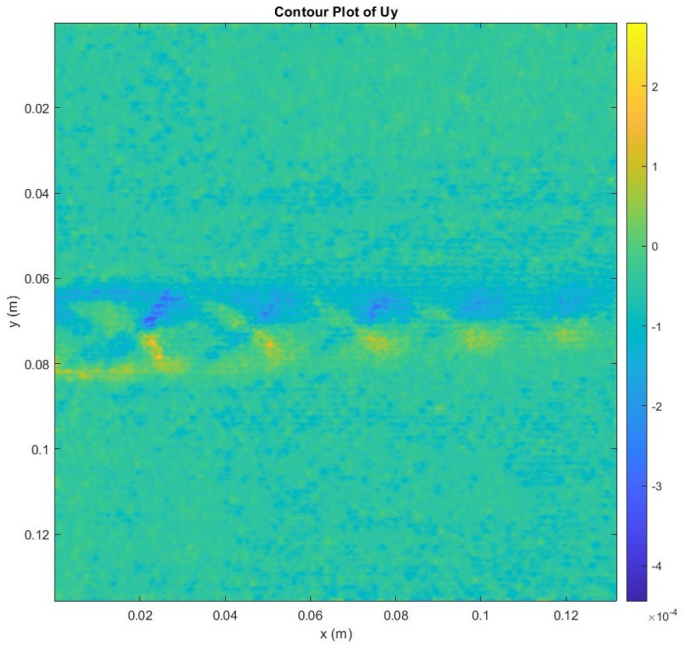

Figure 4.32: Pixel displacement in y-direction for nozzle flow using optical flow

Total displacement

The total pixel displacement using the optical flow algorithm is shown in the figure 4.33.

The maximum pixel displacement in the x-direction was $4.92 \times 10^{-4}m$ while the minimum pixel displacement was $5.58 \times 10^{-8}m$.

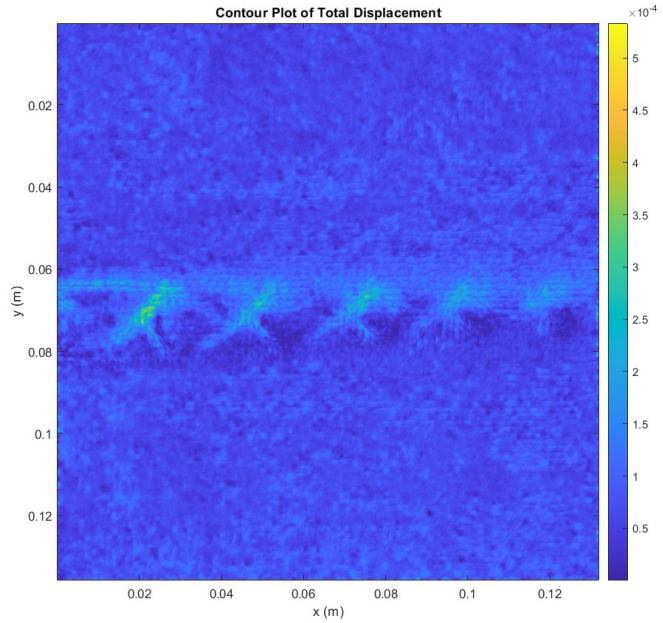

Figure 4.33: Total pixel displacement for nozzle flow using optical flow

The results obtained from the optical flow show the shock diamond pattern only in the region of the flow from the nozzle. The values besides the nozzle flow show zero displacement value and it is expected since the intensity changes only in the region where the flow is occurring.

Results from Hybrid Algorithm

Displacement in x-direction

The pixel displacement in the x direction using the hybrid algorithm is shown in the figure 4.34.

The maximum pixel displacement in the x-direction was $9.91 \times 10^{-5}m$ while the minimum pixel displacement was $-2.57 \times 10^{-4}m$.

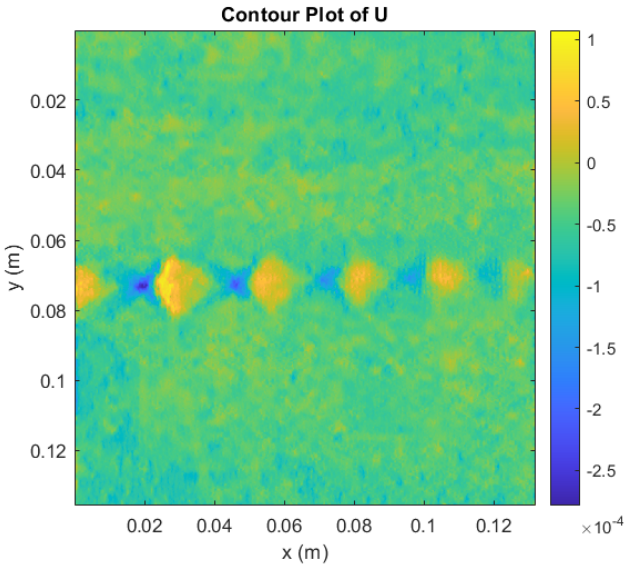

Figure 4.34: Pixel displacement in x-direction obtained using hybrid algorithm

Displacement in y-direction

The pixel displacement in the y direction using the hybrid algorithm is shown in figure 4.35.

The maximum pixel displacement in the y-direction was $1.18 \times 10^{-4}m$ while the minimum pixel displacement was $-2.44 \times 10^{-4}m$.

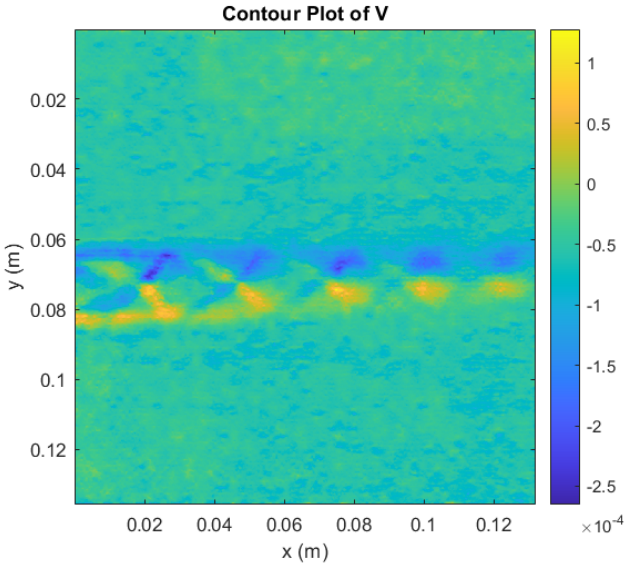

Figure 4.35: Pixel displacement in y-direction obtained using hybrid algorithm

Total displacement

The total pixel displacement using the hybrid algorithm is shown in figure 4.36.

The maximum pixel displacement was $2.83 \times 10^{-4}m$ while the minimum pixel displacement was $5.42 \times 10^{-7}m$.

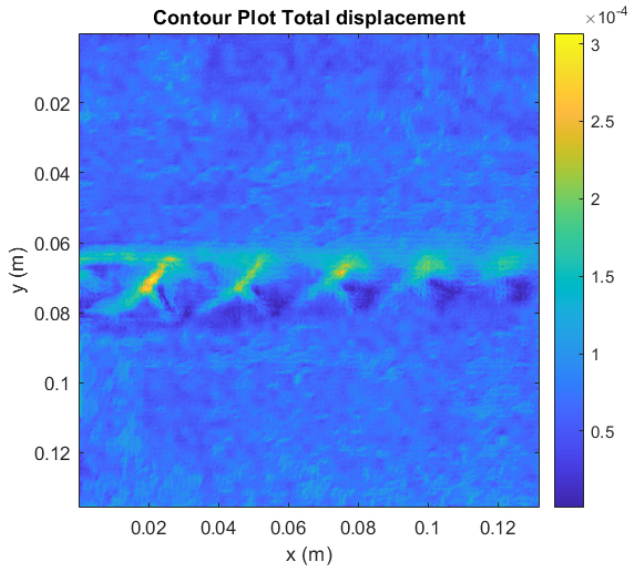

Figure 4.36: Total pixel displacement obtained using hybrid algorithm

4.1.5 Error Analysis

The error analysis of individual algorithms should be carried out in order to weigh out their strength sand weaknesses. The relevance of hybrid method and its implementation is only justified when the error analysis is done.

The validity of the hybrid algorithm is established through a thorough comparison of measurements across various BOS imaging scenarios. These scenarios included standard image that includes small as well as large displacements. By encompassing such diverse scenarios, the comparison provides a comprehensive evaluation of the hybrid algorithm's performance across different conditions. This approach ensures that the method's efficacy is not limited to specific scenarios but extends to a range of real-world applications, thereby enhancing its credibility and applicability in practical settings.

Synthetic BOS Image

The synthetic BOS image represents the optimal image type that can typically be captured during experimental procedures. The reference synthetic image is shifted by 2 pixels in both x and y directions, in order to obtain the shifted image. This shifted image is later fed into each algorithm along with the hybrid algorithm. Given the known displacement, the absolute error is determined for displacements in x and y direction. The images used for the analysis are shown in figure 4.37.

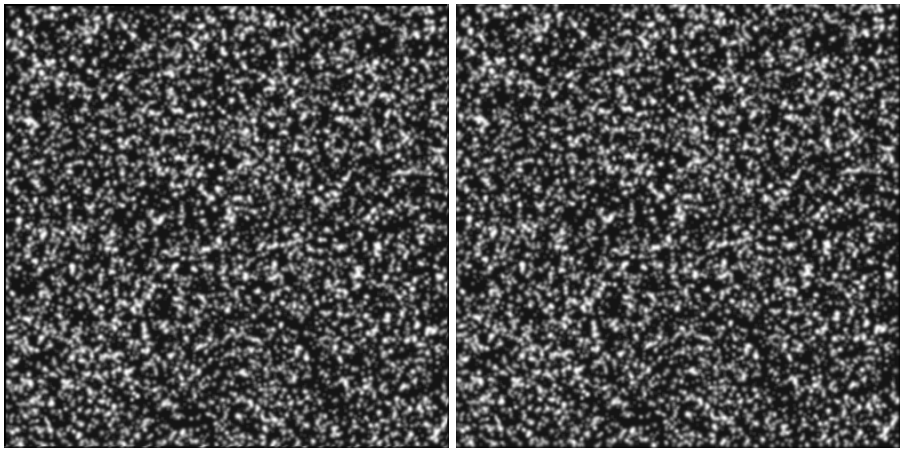

(a) Reference image (b) Shifted image

Figure 4.37: Synthetic images for error analysis

Cross-Correlation Error

In cross-correlation method clusters of pixels in the image domain are taken in-order to identify the correlation peak. The size of the interrogation window and the search region directly affect the results obtained from the cross-correlation algorithm as was seen previously.

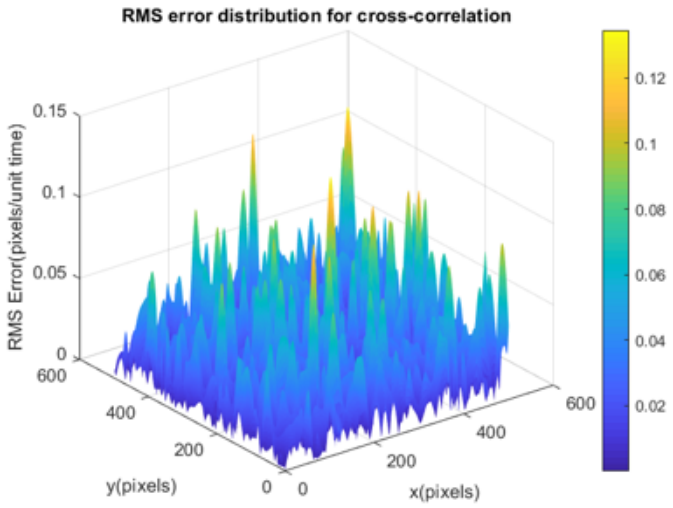

(a) RMS error distribution for cross-correlation

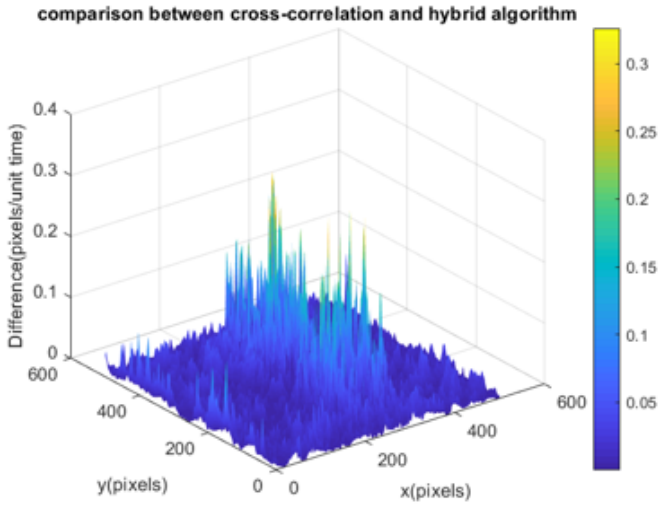

(b) Comparison between cross-correlation and hybrid algorithm

Figure 4.38: Error analysis of results from cross-correlation algorithm

Optical Flow Error

As the underlying principle of the optical flow method is brightness constancy also referred as the "brightness constraint", it is very critical to incorporate the intensity gradient with respect to time as the large component of the error. If there's a discrepancy in intensity gradient between the reference and distorted images, it significantly affects the comparison of these gradients. Another critical aspect is the intensity gradient in

the x- and y-directions. Any introduced error along these coordinates can lead to inaccurate results due to the impact on the intensity gradient. Additionally, changes in the velocity gradient contribute significantly to errors, as they reflect the ability to adhere to the smoothness constraint. Liu et al established that the errors in optical flow tend to increase with displacement increments, as the solution of the time derivative becomes less accurate [52]. However, for very small displacements, the optical flow method performs well, especially when dealing with nearly continuous patterns.

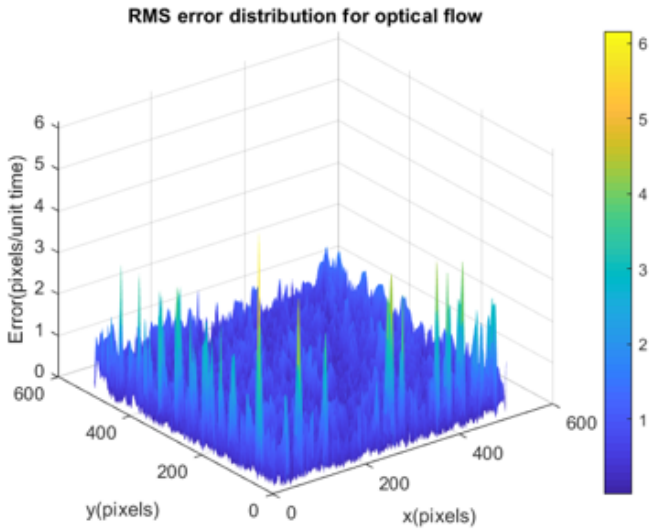

(a) RMS error distribution for optical flow algorithm

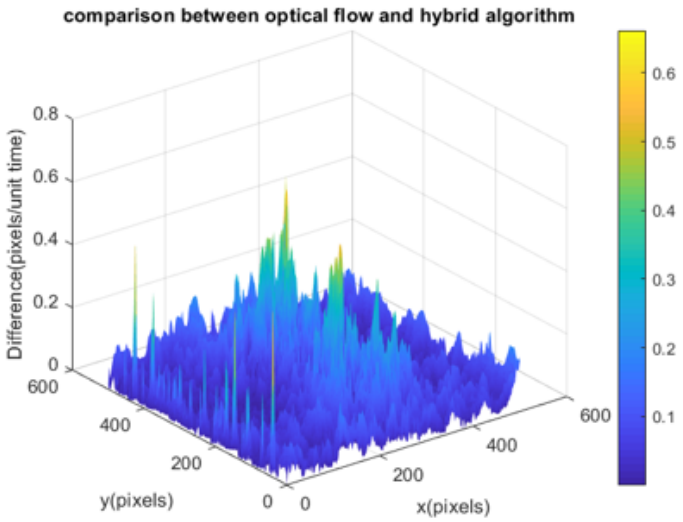

(b) Comparison between optical flow and hybrid algorithm

Figure 4.39: Error analysis of results from optical flow algorithm

Hybrid Algorithm Error

The validity of the hybrid algorithm is established through a thorough comparison of measurements across various BOS imaging scenarios.

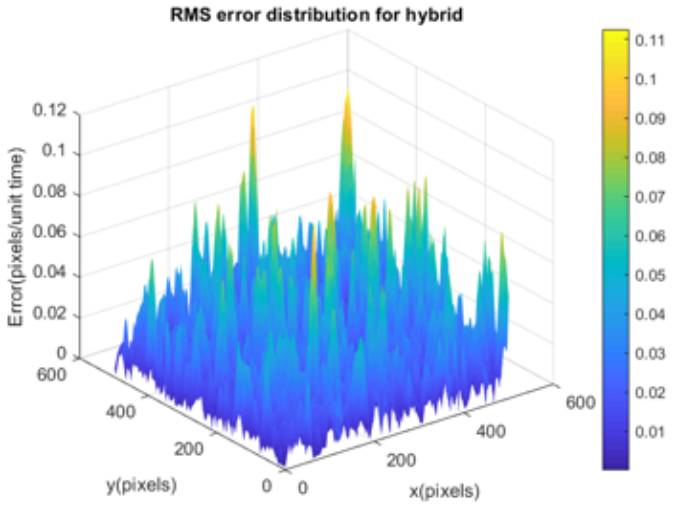

Figure 4.40: RMS error distribution for hybrid algorithm

The displacement in the x-direction error plots above highlights that the hybrid algorithm exhibits lower error rates. However, the optical flow algorithm demonstrates poorer performance near the boundaries since the image is shifted by 2 pixels in both the x and y direction and the the discrepancies are only in boundaries, with comparable error distribution in other regions. Similarly, for the displacement in the y-direction, the hybrid algorithm shows relatively low error rates. The hybrid method generally outperforms both the cross-correlation method and optical flow method across most regions, although it occasionally yields errors similar to those of cross-correlation.

These plots illustrate how the macro component of the displacement vector is derived from the correlation method, while the finer vector is determined through optical flow. Combining these vectors yields a more accurate displacement field. Theoretically, the integration of optical flow should diminish errors, as verified by subsequent error plots.

This trend also holds true for the calculated displacement in y-direction, as depicted in the subsequent figures 4.38, 4.39, 4.40.

4.1.6 Poisson Solver

The density dynamics of the unit test setup and shock diamond are studied by estimating the density field from the developed Poisson solver. Validation and uses of the Poisson solver are described in this section. The methodology of operation of the Solve Poisson algorithm is described in section 3.5.

Validation of Poisson Solver

To validate the algorithm of the Poisson solver, a reference image has been fed into the program. A function for the given image that will satisfy the Poisson equation has been calculated. Starting with an initial guess of zero the function has been used in equation 3.29 and iterated until satisfactory results are obtained.

Let $Ax = S$ be a system of the n linear equation for the Poisson equation.

where A is a coefficient matrix, S is the source term of the Poisson equation and x is the image matrix.

Assuming $\Delta x = \Delta y$, the Source term can be calculated as,

$$S_{i,j} = \frac{(X\_exact_{i+1,j} + X\_exact_{i-1,j} + X\_exact_{i,j+1} + X\_exact_{i,j-1} - 4X\_exact_{i,j})}{\Delta x^2} \tag{4.31}$$

Figure 4.41: Original Image

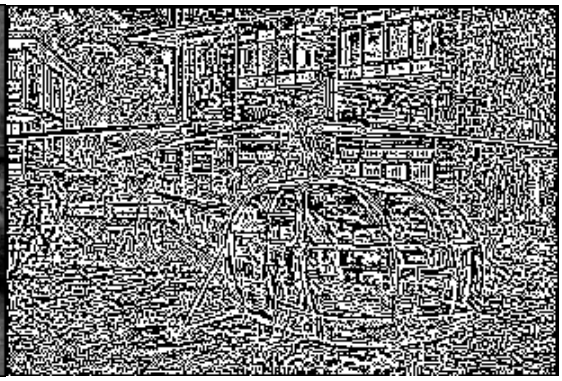

Figure 4.42: Function

(a) 5000 iteration (b) 10000 iteration

(c) 20000 iteration

Figure 4.43: Results from Poisson solver

Above are the results obtained from the Poisson solver with 5000, 10000, and 20000 iterations. As the iteration number is increased the image thus obtained tends to resemble the original image suggesting the solution is converging. The relative error for 5000, 10,000, and 20,000 iterations are 0.1827, 0.0788, $5.36 * 10^{-4}$ respectively.

Density Estimation of Unit Test Subject

The developed Poisson solver is used to estimate the density data of the unit test setup. The parameters used for the density estimation are listed in table 4.5.

Table 4.5: Parameters for density estimation using Poisson solver

Gladstone-Dale constant for air (G)	$2.26e-4m^3/kg$
Distance between background and lens(Z_B)	0.605 m
Magnification(M)	1.2
Refractive index of ambient air (n_0)	1.00029

The boundary conditions employed in the Poisson solver involve:

1. Top and Bottom Boundaries: Neumann Boundary Conditions; $\frac{\partial n}{\partial x} = 0$

2. Left and Right Boundaries: Dirichlet Boundary Conditions

For the experiment conducted at the ambient temperature of 17^0C, the density of the ambient air is $1.07kg/m^3$. Hence, the Dirichlet boundary condition is $\rho_0 = 1.07kg/m^3$.

Density estimation using displacement from cross-correlation algorithm

The contour plot of density estimation using the cross-correlation algorithm is shown in figure 4.44.

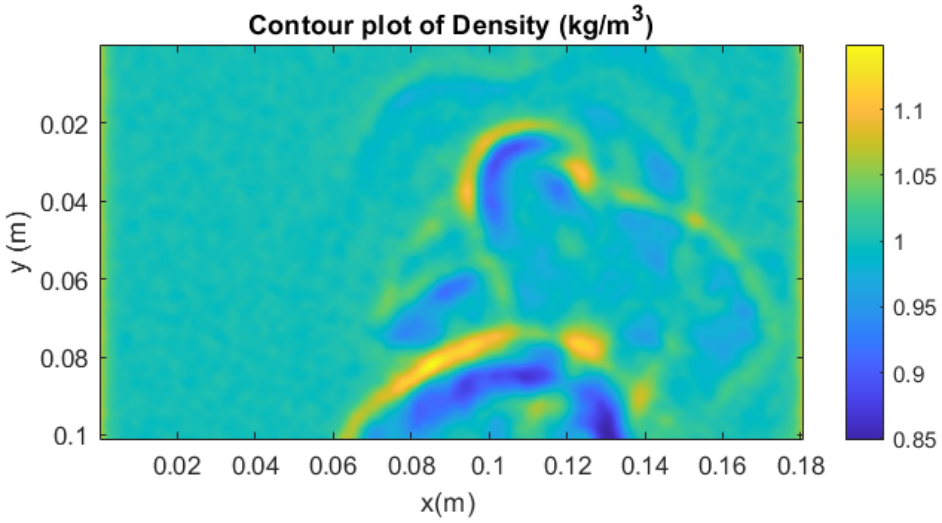

Figure 4.44: Density estimation using displacement from cross-correlation algorithm

Density estimation using displacement from optical flow algorithm

The contour plot of density estimation using the optical flow algorithm is shown in figure 4.45

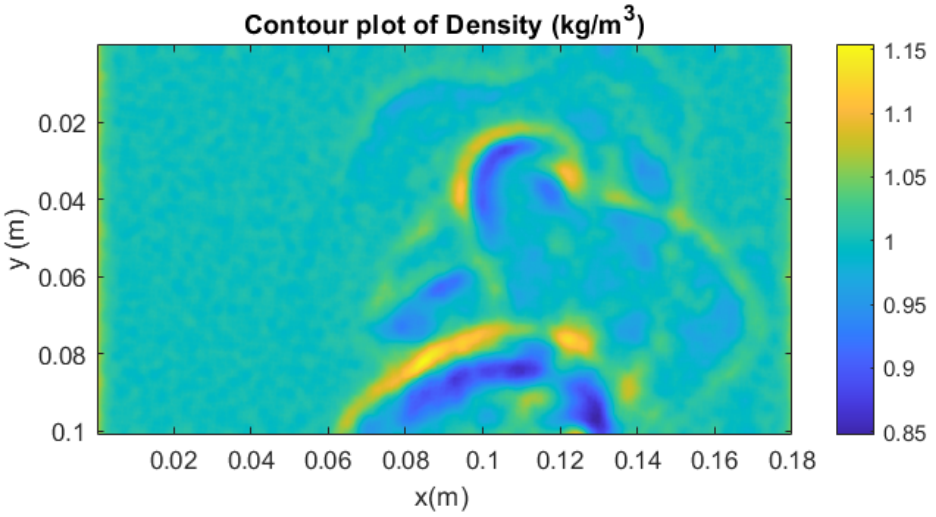

Figure 4.45: Density estimation using displacement from optical flow algorithm

Density estimation using displacement from hybrid algorithm

The contour plot of density estimation using the hybrid algorithm is shown in figure 4.46.

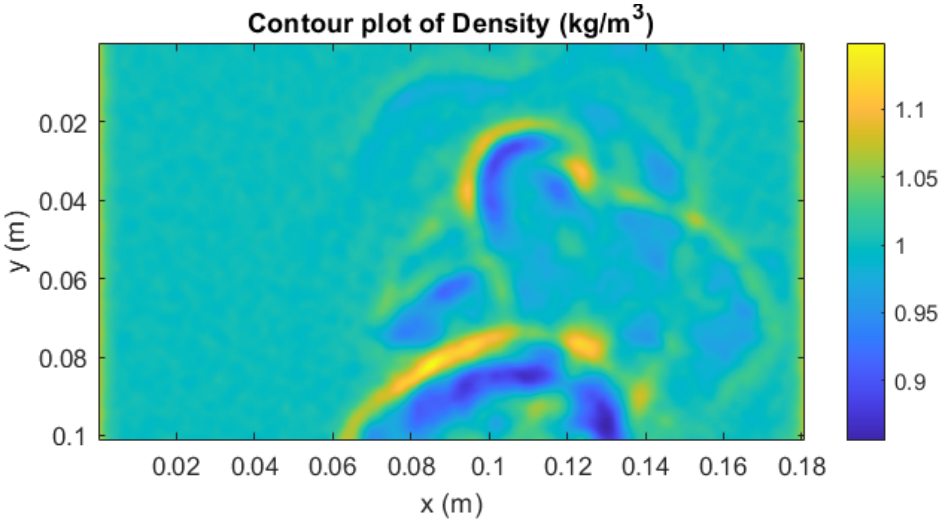

Figure 4.46: Density estimation using displacement from hybrid algorithm

Density Estimation of Main Test Subject

The developed Poisson solver is used to estimate the density data of the shock diamonds of the flow from the under-expanded nozzle. The parameters used for the density estimation are listed in table 4.6.

Table 4.6: Parameters for density estimation using Poisson solver

Gladstone-Dale constant for air (G)	$2.26e-4m^3/kg$
Distance between background and lens(Z_B)	0.285 m
Magnification(M)	2.7
Refractive index of ambient air (n_0)	1.00029

The boundary conditions employed in the Poisson solver involve:

1. Left and Right Boundaries: Neumann Boundary Conditions; $\frac{\partial n}{\partial x} = 0$
2. Top and Bottom Boundaries: Dirichlet Boundary Conditions

For the experiment conducted at the ambient temperature of 16^0C, the density of the ambient air is $1.225kg/m^3$. Hence, the Dirichlet boundary condition is $\rho_0 = 1.225kg/m^3$.

Density estimation using displacement from cross-correlation algorithm

The contour plot of density estimation using the cross-correlation algorithm is shown in figure 4.47.

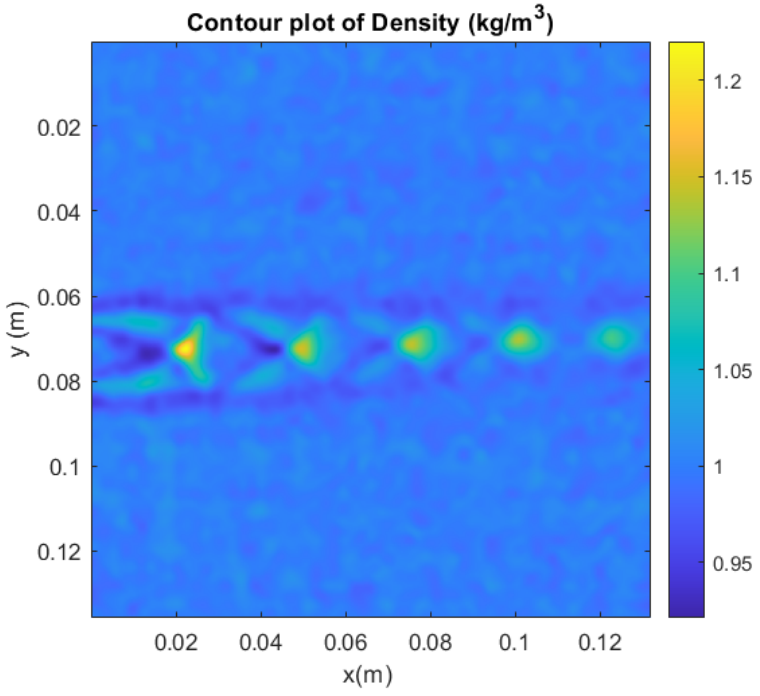

Figure 4.47: Density estimation using displacement from cross-correlation algorithm

Density estimation using displacement from optical flow algorithm

The contour plot of density estimation using the optical flow algorithm is shown in figure 4.48

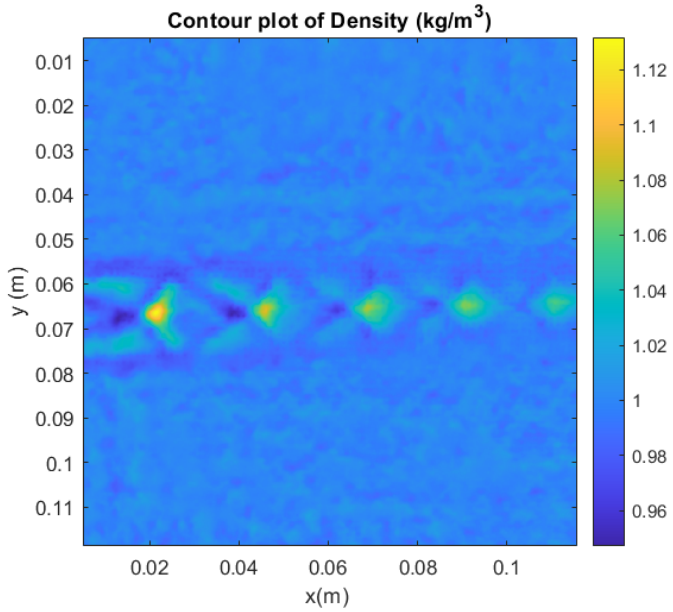

Figure 4.48: Density estimation using displacement from optical flow algorithm

Density estimation using displacement from hybrid algorithm

The contour plot of density estimation using the hybrid algorithm is shown in figure 4.49.

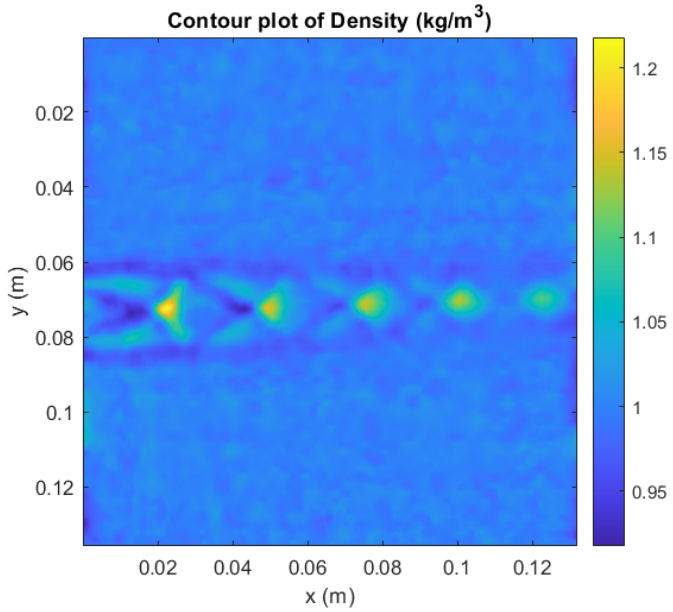

Figure 4.49: Density estimation using displacement from hybrid algorithm

4.2 Work Completed

The overall tasks for this project were divided into various categories as follows:

1. Development of a program for cross-correlation algorithm
2. Development of a program for optical flow algorithm
3. Hybridization of cross-correlation and optical flow algorithm
4. Density distribution estimation using Poisson solver
5. Setup formulation

We have completed the development of a program for both cross-correlation as well as an optical flow algorithm and a Poisson solver for density estimation. The necessary comparison for both cross-correlation, as well as optical flow algorithms, has also been carried out as required. All of the required programs were formulated using MATLAB. After weighing out the pros and cons of the cross-correlation and optical flow algorithm individually, both algorithms were integrated together to generate hybrid algorithm. Various setup arrangements were also created to perform tests which included randomly generated speckle patterns behind test subjects such as nozzle, candle etc. The results are evaluated using the data obtained from these setups using cross-correlation, optical flow and hybrid algorithms.

4.3 Limitations

- The algorithm thus developed can be used only for the flow in which there is a sufficient density gradient. Thus the algorithm can be used for supersonic flow in which there is considerable change in density gradient due to the compressibility effect or in flow where there is heating phenomena, as in convection, which results in the change in the density due to temperature variation. We have not been able to demonstrate the usage of the developed algorithm in the case of the subsonic isothermal flows.

- The program is tailored for application in flow visualization using BOS. However, it is not yet ready-to-use software and requires several refinements and validations before it can be deployed effectively. These refinements and validations are essential to ensure the accuracy, reliability, and usability of the program in real-world scenarios.

- The current study only focuses on 2D flow visualization considering the resources available for the study. 3D flow visualization using BOS is called tomographic background oriented schlieren and this 3D visualization requires large number of cameras triggered simultaneously at same instant of time.

4.4 Problems Encountered

The problems faced during the project are as follows:

1. Setup construction

   The optical setup construction in the case of the BOS experiment is a hit-and-trial process, a prior construction of setup isn't practical. The factors like camera resolution, frame rate, and light intensity among others affect the image acquisition process. Optimizing each of the variables is a humongous task in itself. Though, what we have achieved in the limited time frame in regards to the setup construction is commendable yielding accurate pixel displacement (up to the first decimal place) the setup could be further optimized for more sensitive flow measurements.

2. Validation of test results

   The result obtained from the BOS experiment using the in-house code is closely aligned with those obtained from other processing software that uses similar image processing techniques. Unfortunately, there aren't many openly available software that are used specifically for BOS, most of them being created for PIV image analysis. Furthermore, even though some of the flow characteristics can and have been validated quantitatively, extensive instruments are required for other measurements to obtain ground truth

data for example measuring the density field of the flow. Thus we were technologically limited in validating the results that we obtained from our analysis.

4.5 Budget Analysis

The total budget breakdown of finance invested during this project is presented in the table 4.7.

Table 4.7: Budget Analysis

S.N.	Particulars	Amount	Remarks
1	High Speed Camera	$7000	Was available in "Flow Visualization Lab" in DMAE
2	Variable Intensity Light Source	NRs. 19000	Was available in "Flow Visualization Lab" in DMAE
3	Computational Cost	NRs. 30000	
4	Documentation	NRs. 7000	
5	Miscellaneous	NRs. 10000	
Total		NRs.47000	

The project was mostly based on code development. Thus the total budget of NRs. 47,000 was expended during the project including the computational cost, documentation, and miscellaneous expenses. The already available resources have not been included as an expense in the total budget. However, if one has to undergo, a similar study, the expenses that are required in the study should include the cost of a high-speed camera and variable-intensity light source.

CHAPTER 5: CONCLUSION AND FUTURE ENHANCEMENT

5.1 Conclusion

The study aimed at measurement of the flow parameters using the Background Oriented Schlieren. A tool was developed using the cross-correlation and optical flow algorithm for obtaining the displacement of the background pixels, and the Poisson solver was used for estimating the density using the displacements thus obtained. Furthermore, the hybrid algorithm was developed by combining cross-correlation and the optical flow algorithm providing us with a more refined displacement field. The study demonstrated the successful implementation of the developed hybrid algorithm to process BOS images and obtain density fields.

For the test subjects synthetic image, the hot plume from the candle and under-expanded flow from the nozzle were selected. The displacement data were used for visualizing the flow and for constructing the density field of the flow. The obtained displacement data was cross-checked with the displacements produced by the commercially available PIV image processing software (PIVLab), and the two results agreed with each other closely.

Background-oriented schlieren is a powerful technique that can be used for making the quantitative as well as the qualitative measurements of the flow. The technique is non-intrusive, inexpensive and yields accurate results as compared to other techniques used. Furthermore, the ability to measure various flow parameters in extension to density can be a crucial tool for researchers studying various flow and heat transfer phenomena.

5.2 Scope for Future Enhancement

- The accuracy of Horn and Schunck's optical flow algorithm is defined by the regularization parameter λ. The regularization parameter is being determined using the extensive hit-and-trial method for specific applications. The current study can be further improved by providing a method to determine these parameters using

synthetic images generated for a particular application.

- Optical flow algorithms such as Lucas-Kanade algorithm, Brox algorithm, Farneback algorithm can be implemented and comparative study can be carried out to rule out their pros and cons as opposed to Horn and Schunck algorithm.

- For the cross-correlation algorithm, currently direct cross-correlation (DCC) has been used. Though DCC has been widely studied and used in many research experiments, newer algorithms are being developed that are more robust and accurate. The current study can be improved by using other correlation techniques as well [32] [33].

- Although an attempt to undergo the error analysis of the developed hybrid method is done, the overall accuracy and error metrics of the algorithm used in this study are yet to be completely studied. The analysis of accuracy and error should be done to determine the usability of the algorithm in various applications and test subjects.

- Besides synthetic image validation, rigorous validation of the displacement estimation algorithms and Poisson solver is yet to be done. For example, in the visualization of shock waves, resulting flow parameters such as temperature, pressure, and density can be validated using the analytical solution or using CFD simulations.

References

[1] M. Raffel, C. E. Willert, F. Scarano, C. J. Kähler, S. T. Wereley, and J. Kompenhans, *Particle Image Velocimetry*. Springer International Publishing, 2018.

[2] T. Liu, A. Merat, M. Makhmalbaf, C. Fajardo, and P. Merati, "Comparison between optical flow and cross-correlation methods for extraction of velocity fields from particle images," *Experiments in Fluids*, vol. 56, pp. 1–23, 2015.

[3] S. Maharjan, "Design and setup of z-type schlieren imaging system for flow visualization," 2023.

[4] L. M. Weinstein, "Large-field high-brightness focusing schlieren system," *AIAA journal*, vol. 31, no. 7, pp. 1250–1255, 1993.

[5] L. Weinstein, "Large field schlieren visualization-from wind tunnels to flight," *Pro. Of VSJ-SPIE98.,(1998)*, pp. 1–12, 1998.

[6] L. Becher, C. Voelker, V. Rodehorst, and M. Kuhne, "Background-oriented schlieren technique for two-dimensional visualization of convective indoor air flows," *Optics and Lasers in Engineering*, vol. 134, 11 2020.

[7] D. Ramanah and D. Mee, "Scramjet flow visualization using background oriented schlieren in hypersonic impulse facilities," in *14th AIAA/AHI space planes and hypersonic systems and technologies conference*, p. 8004, 2006.

[8] Q. Zhong, H. Yang, and Z. Yin, "An optical flow algorithm based on gradient constancy assumption for piv image processing," *Measurement Science and Technology*, vol. 28, no. 5, p. 055208, 2017.

[9] T. Liu and D. M. Salazar, "Openopticalflow_piv: an open source program integrating optical flow method with cross-correlation method for particle image velocimetry," *Journal of Open Research Software*, vol. 9, no. 1, 2021.

[10] S. á. Dalziel, G. O. Hughes, and B. R. Sutherland, "Whole-field density measurements by 'synthetic schlieren'," *Experiments in fluids*, vol. 28, no. 4, pp. 322–335, 2000.

[11] B. Atcheson, W. Heidrich, and I. Ihrke, "An evaluation of optical flow algorithms for background oriented schlieren imaging," *Experiments in fluids*, vol. 46, pp. 467–476, 2009.

[12] L. Venkatakrishnan and G. E. A. Meier, "Density measurements using the background oriented schlieren technique," *Experiments in Fluids*, vol. 37, pp. 237–247, 8 2004.

[13] G. Vasudeva, D. R. Honnery, and J. Soria, "Non-intrusive measurement of a density field using the background oriented schlieren (bos) method," in *Proc. Australian Conf. Laser Diagnostic in Fluid Mechanics & Combustion*, 2005.

[14] H. Huang, D. Dabiti, and M. Gharib, "On errors of digital particle image velocimetry," *Measurement Science and Technology*, 1997.

[15] S. Okamoto, Nishio and Kobayashi, "Standard images for the particle-image velocimetry," *Measurement Science and Technology*, 2000.

[16] D. Lyon, "The discrete fourier transform, part 6: Cross-correlation," *The Journal of Object Technology*, 2010.

[17] *Sub-Pixel image interpolation for PIV*, 2004.

[18] D. Fleet and Y. Weiss, "Optical flow estimation," in *Handbook of mathematical models in computer vision*, pp. 237–257, Springer, 2006.

[19] B. K. Horn and B. G. Schunck, "Determining optical flow," *Artificial intelligence*, vol. 17, no. 1-3, pp. 185–203, 1981.

[20] H. Richard and M. Raffel, "Principle and applications of the background oriented schlieren (bos) method," *Measurement science and technology*, vol. 12, no. 9, p. 1576, 2001.

[21] G. Meier, "Computerized background-oriented schlieren," *Experiments in fluids*, vol. 33, no. 1, pp. 181–187, 2002.

[22] R. Adrian, "Statistical properties of particle image velocimetry measurements in turbulent flow," *Laser Anemometry in Fluid Mechanics*, 1988.

[23] N. T. Smith, J. T. Heineck, and E. T. Schairer, "Optical flow for flight and wind tunnel background oriented schlieren imaging," in *55th AIAA aerospace sciences meeting*, p. 0472, 2017.

[24] K. Kindler, E. Goldhahn, F. Leopold, and M. Raffel, "Recent developments in background oriented schlieren methods for rotor blade tip vortex measurements," *Experiments in Fluids*, vol. 43, pp. 233–240, 2007.

[25] H. A. Ghazwani, "Preliminary study of optical-flow based background-oriented schlieren measurements," 2016.

[26] S. Raghunath, D. J. Mee, T. Roesgen, and P. A. Jacobs, "Visualization of supersonic flows in shock tunnel, using the background oriented schlieren technique."

[27] J. tipnis, M. V. F. mvfinnis, cranfieldacuk K Knowles, and D. bray, "Density measurements for rectangular free jets using background-oriented schlieren," 2013.

[28] K. Hayasaka, Y. Tagawa, T. Liu, and M. Kameda, "Optical-flow-based background-oriented schlieren technique for measuring a laser-induced underwater shock wave," *Experiments in Fluids*, vol. 57, pp. 1–11, 2016.

[29] O. Léon, G. L. Besnerais, L. Lanzillotta, and D. Donjat, "3d density reconstruction of a screeching supersonic jet by synchronized multi-camera background oriented schlieren.," 2019.

[30] F. Nicolas, D. Donjat, O. Léon, G. L. Besnerais, F. Champagnat, and F. Micheli, "3d reconstruction of a compressible flow by synchronized multi-camera bos," vol. 58, p. 2017.

[31] X. ye and X. Niu, "Optimization in piv algorithm for visualizing vortices in bubble wake," *Flow Measurement and Instrumentation*, 2022.

[32] B. Shi, J. Wei, and M. Pang, "A modified cross-correlation algorithm for piv image processing of particle-fluid two-phase flow," *Flow Measurement and Instrumentation*, 2015.

[33] T. Earl, Y. J. Jieon, B. Lecordier, and L. David, "F2dpr:a fast and robust cross-correlation technique for volumetric piv," *Measurement Science and Technology*, 2016.

[34] M. Raffel, C. Tung, H. Richard, Y. Yu, and G. Meier, "Background oriented stereoscopic schlieren (boss) for full-scale helicopter vortex characterization," 2000.

[35] L. Becher, C. Voelker, V. Rodehorst, and M. Kuhne, "Background-oriented schlieren technique for two-dimensional visualization of convective indoor air flows," *Optics and Lasers in Engineering*, 2020.

[36] F. Nicolas, D. Donjat, O. Leon, G. L. Besnerais, F. Champagnat, and F. Micheli, "3d reconstruction of a compressible flow by synchronized multi-camera bos," *Experiment in Fluids*, vol. 58, 2017.

[37] A. Aminfar, J. Cobian-Iñiguez, M. Ghasemian, N. Rosales Espitia, D. R. Weise, and M. Princevac, "Using background-oriented schlieren to visualize convection in a propagating wildland fire," *Combustion Science and Technology*, vol. 192, no. 12, pp. 2259–2279, 2020.

[38] B. O. Cakir, S. Lavagnoli, B. H. Saracoglu, and C. Fureby, "Assessment and application of optical flow in background-oriented schlieren for compressible flows," *Experiments in Fluids*, vol. 64, no. 1, p. 11, 2023.

[39] K. Jambunathan, X. Ju, B. Dobbins, and S. Ashforth-Frost, "An improved cross correlation technique for particle image velocimetry," *Measurement Science and Technology*, vol. 6, no. 5, p. 507, 1995.

[40] Z. Yang and M. Johnson, "Hybrid particle image velocimetry with the combination of cross-correlation and optical flow method," *Journal of Visualization*, vol. 20, pp. 625–638, 2017.

[41] J. H. Seong, M. S. Song, D. Nunez, A. Manera, and E. S. Kim, "Velocity refinement of piv using global optical flow," *Experiments in Fluids*, vol. 60, pp. 1–13, 2019.

[42] L. Venkatakrishnan, "Density measurements in an axisymmetric underexpanded jet by background-oriented schlieren technique," *AIAA Journal*, vol. 43, pp. 1574–1579, 7 2005.

[43] E. Goldhahn and J. Seume, "The background oriented schlieren technique: sensitivity, accuracy, resolution and application to a three-dimensional density field," *Experiments in Fluids*, vol. 43, pp. 241–249, 8 2007.

[44] D. Ramanah, S. Raghunath, D. J. Mee, T. Rösgen, and P. A. Jacobs, "Background oriented schlieren for flow visualisation in hypersonic impulse facilities," *Shock Waves*, vol. 17, pp. 65–70, 8 2007.

[45] L. Venkatakrishnan and P. Suriyanarayanan, "Density field of supersonic separated flow past an afterbody nozzle using tomographic reconstruction of bos data," *Experiments in Fluids*, vol. 47, pp. 463–473, 9 2009.

[46] K. Heng, *Exoplanetary Atmospheres*. Princeton University Press, 2017.

[47] C. Robinson, "Flow through a de laval nozzle," 2016.

[48] B. Gautam, K. Budahthoki, and M. Sitoula, "Supersonic nozzle test using high pressure compressor," 4 2023.

[49] G. S. Settles, "Schlieren and shadowgraph techniques."

[50] S. Yousef, *Iterative Methods for Sparse Linear Systems*. 3 ed., 1 2000.

[51] K. Okamoto, S. Nishio, T. Saga, and T. Kobayashi, "Standard images for particle-image velocimetry," *Measurement Science and Technology*, vol. 11, no. 6, p. 685, 2000.

[52] T. Liu and L. Shen, "Fluid flow and optical flow," *Journal of Fluid Mechanics*, vol. 614, pp. 253–291, 2008.

APPENDICES

APPENDIX A: SOURCE CODE FOR HYBRID ALGORITHM WRITTEN IN MATLAB

The source code corresponding the code developed is hosted on GitHub and included in the repository below;
`https://github.com/group-9-BOS/Hybrid-BOS.git`

Feedback and suggestions are welcome and greatly appreciated, as it help improve the project for everyone. It is encouraged to browse the code, submit issues, and even contribute to the project if they are interested. Any input from the community will be valued and acknowledged.

For any issues, suggestion or request for access feel free to reach out at;

Nimesh Chaulagain: 076bas022.nimesh@pcampus.edu.np

Samiksha Dhakal: 076bas033.samiksha@pcampus.edu.np

Shushant Poudel: 076bas042.shushant@pcampus.edu.np

Sushil Pandey: 076bas044.sushil@pcampus.edu.np

APPENDIX B: QUALITATIVE COMPARISON

A qualitative comparison of the results from BOS with Z-type Schlieren visualization of under-expanded flow from nozzle is shown in the figure.

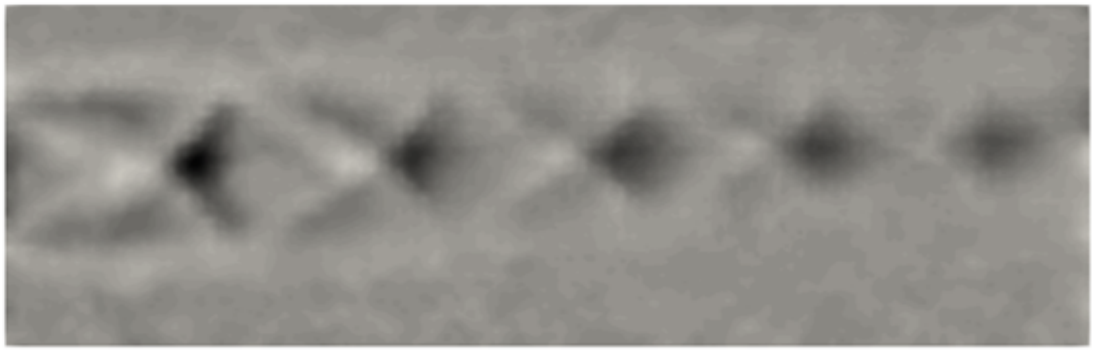

(a) BOS visualization after density reconstruction

(b) Z-type Schlieren visualization [3]

Figure: Qualitative comparison of shock diamond